LU-TP 21-07
January 2021

Searching for signatures of compositeness of the Higgs boson

Mårten Bertenstam

Department of Astronomy and Theoretical Physics, Lund University

Master thesis supervised by Roman Pasechnik and Johan Rathsman

LUND
UNIVERSITY

Abstract

In this master thesis we consider some phenomenological aspects of two-Higgs-doublet models, both elementary and composite ones. The emphasis is on calculating and understanding first order phase transitions in such models, constrained to be in agreement with existing collider data on the Higgs sector. We also consider the contribution to the gravitational wave background of the universe that would originate from such phase transitions, in order to investigate whether the models could be probed through the LISA, BBO and DECIGO gravitational wave detectors that are being planned. As a proof of concept, we find that we can generate model realizations with such first order phase transitions in both elementary and composite models. In the elementary case, we find at least a few benchmark points that would be in the observable range of LISA. However, more data would be needed to properly investigate correlations between the gravitational wave signals and other aspects of the models, such as the collider phenomenology.

Populärvetenskaplig beskrivning

Att föremål har massa är inte någonting vi ifrågasätter i det vardagliga livet. Att förstå *varför* materiens minsta byggstenar, elementarpartiklarna, har massa är däremot inte så enkelt. I standardmodellen, som utgör den fysikaliska beskrivningen för naturens allra minsta beståndsdelar, spelar den så kallade Higgsmekanismen en avgörande roll för att förklara hur elementarpartiklar får massa. Higgsmekanismen i standardmodellen förutsäger existensten av en ny partikel, den så kallade Higgsbosonen. Genom dess upptäckt år 2012 i partikelacceleratorn LHC (Large Hadron Collider) i CERN var standardmodellen i någon mening fullbordad.

Samtidigt lämnar standardmodellen många frågor obesvarade, till exempel den om varför universum innehåller så ohyggligt mycket mer materia än antimateria. En annan fråga rör massan hos Higgsbosonen själv. Enligt teoretiska argument borde denna massa vara betydligt större än vad experimentella mätningar visar. Dessa problem, och flertalet andra, kan angripas genom att införa ytterligare, nya slags Higgsbosoner i beskrivningen av naturen. En annan infallsvinkel är att beskriva Higgsbosonen eller Higgsbosonerna som sammansatta partiklar, istället för elementarpartiklar. Därigenom kan man på ett naturligt sätt förklara varför den påvisade Higgsbosonen är så lätt.

En intressant aspekt hos sådana utvidgade Higgsmodeller är att de, under vissa förutsättningar, förutsäger en så kallad första ordningens fasövergång i ett mycket tidigt skede av universums början. Denna fasövergång kan liknas vid kokning av vatten, där små bubblor slumpmässigt uppstår, expanderar och kolliderar med varandra. En sådan fasövergång i det tidiga universum skulle vara en viktig pusselbit i att förklara det ovannämnda problemet gällande överskottet av materia jämfört med antimateria i universum. Vad som är särskilt spännande är att en sådan fasövergång, genom bubblornas expansion i det omgivande mediet, skulle kunna ge upphov till så kallade gravitationsvågor. Sådana vågor kan, om de är tillräckligt kraftiga, uppmätas av framtida gravitationsvågsdetektorer. Det föreliggande arbetet syftar till att studera dessa fenomen hos utvidgade Higgsmodeller, och koppla dem till signaler som kanske kan uppmätas i framtida partikelacceleratorexperiment.

Contents

List of acronyms

SM	Standard Model
BSM	Beyond the SM
2HDM	Two-Higgs-doublet model
E2HDM	Elementary two-Higgs-doublet model
CHM	Composite Higgs model
C2HDM	Composite two-Higgs-doublet model
SFOEWPT	Strongly first-order electroweak phase transition
GW	Gravitational wave
vev	Vaccum expectation value
pGB	pseudo Goldstone boson
FCNC	Flavour changing neutral current
SNR	Signal-to-noise ratio
PIS	Peak-integrated sensitivity
PISC	Peak-integrated sensitivity curve
CL	Confidence level

1 Introduction

The Standard Model (SM) of particle physics is a fundamental theory which describes the known elementary particles and their interactions through the electromagnetic, weak, and strong forces [1, 2, 3]. A crucial part of the SM is the Higgs mechanism [4], which explains how the quarks and the charged leptons, as well as the $W^{\pm}$ and Z^0 bosons, acquire mass through interactions with the Higgs field. Following the discovery of the top quark in 1995 [5, 6], the Higgs boson remained the last missing piece of the SM. With the discovery of the Higgs boson at LHC in 2012 [7, 8], the SM was thus complete.

Still, there are strong indications that the SM cannot, ultimately, be the correct fundamental description of nature. For example, an important issue is to explain the nature of dark matter, for whose existence there is ample evidence from cosmology [9]. Moreover, the SM cannot explain the observed baryon asymmetry in the universe, i.e. why there is more matter than anti-matter [10, 11]. Aside from these, there are also issues which are possibly more of an aesthetic nature. These concern the large number of parameters in the SM [1, 3], the unnatural fine-tuning necessary to explain the smallness of the mass of the Higgs boson compared to the Planck mass, and the related hierarchy problem, which refers to the enormous difference in scale between the electroweak force and the gravitational force [3, 12]. Specifically, quantum corrections to the Higgs mass, mainly from top quark loops, would drive the mass of the Higgs boson to the Planck scale, unless the corrections are cancelled by a very large and fine-tuned bare Higgs mass. Several of these issues can be addressed by extending the original Higgs sector.

There are various ways to extend the SM in such a way that the well-tested low-energy predictions of the SM are retained, while addressing some of the issues discussed above. One approach is to introduce another Higgs doublet, yielding the (elementary) two Higgs doublet models (E)2HDM [12, 13]. The addition of a new Higgs doublet leads to a larger number of Higgs bosons, namely the neutral h, H and A, of which h can be interpreted as the SM Higgs boson, as well as the charged $H^{\pm}$. The 2HDM is motivated by the fact it appears in the minimal supersymmetric (SUSY) extension (MSSM) of the SM [14]. The stop quark, i.e. the spin-1 superpartner of the top quark in SUSY, cancels the quantum corrections to the Higgs mass from the top quark, and thereby solves the fine tuning problem mentioned above. While the LHC has so far not found any evidence for supersymmetry [15], the E2HDM is still a worthwhile subject of study. For example, it can address the baryon asymmetry problem [16].

An alternative solution to the fine-tuning problem is offered by composite Higgs models (CHMs) [17, 18] and, in particular, by composite two Higgs doublet models (C2HDM) [19]. In these models, the Higgs bosons are no longer elementary particles, but rather bound states of a new type of strong interaction. In a particular setting of the composite Higgs models, the Higgs bosons are realized as pseudo Goldstone bosons (pGBs) by the spontaneous breaking of a global symmetry. Unlike in the SM, this global symmetry is not exact but explicitly broken, which is needed in order for the Goldstone modes to be massive. Through this mechanism, the mass of lightest Higgs boson can be kept small without invoking fine-tuning, thus solving the fine-tuning problem of the Higgs mass [19].

As was mentioned above, one of the shortcomings of the SM is its failure to explain the overwhelming abundance of matter (baryons) versus antimatter (antibaryons). This constitutes the so-called baryon asymmetry problem, and the process in the early universe that produced the observed baryon asymmetry is referred to as baryogenesis [10]. In 1967, Sakharov [20] formulated the following three necessary conditions for baryogenesis to take place

1. Baryon number violation
2. Violation of C and CP-symmetry
3. Strong departure from thermal equilibirum

One way to realize the third Sakharov condition is through a strongly first order electroweak phase transition (SFOEWPT) in the early universe. As it turns out, however, the SM does not allow, with the observed Higgs mass, a strong enough phase transition to explain the observed baryon asymmetry [10, 11]. Thus, in order to solve the baryon asymmetry problem, we are interested in models which exhibit a strongly first order phase transition.

An interesting feature of a strongly first order phase transition in the early universe is the production of gravitational waves (GW), caused by interactions of the expanding bubbles of the new vacuum phase with the cosmic medium. If strong enough, such gravitational waves could be observed as part of the gravitational wave background (GWB) in the universe. The ongoing development of gravitational wave detectors, notably LISA [21], BBO [22] and DECIGO [23] which are capable of measuring the GWB of the universe, motivates the exploration of particle physics models that can explain the origin of the GWB. Conversely, future measurements of the GWB by such detectors would provide valuable constraints on these models.

In this thesis we investigate some phenomenological aspects of the elementary 2HDM and a particular composite 2HDM, presented in [19] [1]. The philosophy has been to explore different model realizations, i.e. different points in the parameter space, and then apply existing experimental collider constraints to filter out those realizations which are not currently excluded by the available data. Admissible points have then been analyzed with respect to the phase transitions and the resultant gravitational wave signals.

The structure of the thesis is as follows: In section 2, we briefly review the Higgs mechanism in the SM, and then discuss the elementary and composite 2HDM, respectively. Next we discuss phase transitions driven by scalar fields. We first present the effective potential, which is needed to describe the phase transition, and then illustrate the formalism by considering a simplified version of the effective potential in the SM. Thereafter we discuss the dynamics of strongly first order phase transitions, and finally the gravitational wave generation due to this dynamics. In section 3, we discuss the implementation of the models for the numerical investigations that have been performed. In section 4 we present the results of these investigations, and conclude in section 5. Various details which are not covered in the main text are presented in the appendices.

[1] There are different composite 2HDMs, with different symmetry breaking patterns [18].

2 Background

2.1 The Higgs mechanism in the SM

The purpose of this section is to briefly recall the Higgs mechanism [4] in the SM, and to serve as an introduction to the extended Higgs models to be considered below. The Higgs sector in the SM has the form

$$\mathcal{L}_{\text{Higgs}} = (D^\mu \Phi)^\dagger (D_\mu \Phi) - V_{\text{Higgs}}(\Phi), \tag{2.1}$$

where Φ is the complex $SU(2)$ Higgs doublet, D_μ is the gauge covariant derivative, given by

$$D_\mu = \partial_\mu - ig\frac{\tau_a}{2}W_\mu^a - ig'\frac{Y}{2}B_\mu, \tag{2.2}$$

and V_{Higgs} is the Higgs potential, given by

$$V_{\text{Higgs}}(\Phi) = \mu^2 \Phi^\dagger \Phi + \lambda(\Phi^\dagger \Phi)^2. \tag{2.3}$$

By construction, the Higgs Lagrangian in equation 2.1 has a $SU(2) \times U(1)_Y$ symmetry. The $SU(2)$ gauge fields are the W_μ^a fields, which along, with the $SU(2)$ generators τ_a and the coupling g, were introduced in equation 2.2. Similarly, B_μ is the $U(1)_Y$ gauge field, Y is the $U(1)_Y$ generator and g' the associated coupling.

In the Higgs potential, we require that the parameter λ satisfy $\lambda > 0$ in order for the potential to be bounded from below. If the parameter μ^2 satisfies $\mu^2 < 0$, the Higgs potential has a non-trivial degenerate global minimum given by $\Phi^\dagger\Phi = -\mu^2/(2\lambda)$. The minimum is degenerate in the sense that if Φ_0 minimizes the potential, then so does Φ_0' for any Φ_0' obtained by an $SU(2) \times U(1)_Y$ transformation of Φ_0. The physical vacuum state, however, corresponds to one particular value of Φ_0. The vacuum state, therefore, breaks the $SU(2) \times U(1)_Y$ symmetry, while the Lagrangian itself respects the symmetry; this is an example of spontaneous symmetry breaking. Because $\Phi^\dagger\Phi = -\mu^2/(2\lambda) \neq 0$ in the vacuum state, the Higgs field is then said to have acquired a (nonzero) vacuum expectation value (vev) v, given by $v = \sqrt{-\mu^2/\lambda}$.

Let us explicitly write the vacuum Φ_0 in the form $\Phi_0 = (0, v)^T/\sqrt{2}$, which simply amounts to a choice of basis. In this basis, let us consider the charge operator $Q = \tau_3/2 + Y/2$. By assigning the $U(1)$ hypercharge $Y_H = 1$ to the Higgs field, we see that $Q\Phi_0 = 0$, corresponding to charge conservation of the vacuum. Thus, even though the vacuum breaks the $SU(2) \times U(1)_Y$ symmetry, it is still invariant under a $U(1)$ symmetry corresponding to the charge operator Q. We can identify this $U(1)$ symmetry with the $U(1)_{\text{EM}}$ gauge group, and therefore say that the orignal $SU(2) \times U(1)_Y$ symmetry is spontaneously broken down to $U(1)_{\text{EM}}$.

The spectrum of the model can be investigated by expanding around the vacuum value Φ_0 of the Higgs field. Let us write this expansion as

$$\Phi = \frac{1}{\sqrt{2}}\begin{pmatrix} \sqrt{2}G^+ \\ v + h + iG^0 \end{pmatrix}, \tag{2.4}$$

where G^+ is a complex scalar field (with Hermitean conjugate G^-) and where h and G^0 are real fields. If we insert this expansion in equation 2.1 and extract the quadratic part of the h, G^0 and $G^\pm$ fields from the Lagrangian, we obtain

$$\begin{aligned}\mathcal{L}_{\text{Higgs,quad}} &= \frac{1}{2}(\partial_\mu h)(\partial^\mu h) + \frac{1}{2}(\partial_\mu G^0)(\partial^\mu G^0) + (\partial_\mu G^+)(\partial^\mu G^-) \\ &\quad + \left(\frac{3}{2}v^2\lambda + \frac{1}{2}\mu^2\right)h^2 + (v^2\lambda + \mu^2)\left(G^+G^- + \frac{1}{2}(G^0)^2\right) = \\ &= \frac{1}{2}(\partial_\mu h)(\partial^\mu h) + \frac{1}{2}(\partial_\mu G^0)(\partial^\mu G^0) + (\partial_\mu G^+)(\partial^\mu G^-) + v^2\lambda h^2, \end{aligned} \tag{2.5}$$

where, in the last step, we used $\mu^2 = -v^2\lambda$. Thus, we see that the field h is massive, with $m_h^2 = 2v^2\lambda$, while the fields $G^\pm$ and G^0 are massless. The latter fields are the Goldstone bosons associated with the spontaneous symmetry breaking; by Goldstone's theorem [24], one such massless boson appears for each broken group generator.

By an $SU(2)$ transformation (to so-called unitarity gauge), the expansion around the vacuum can be parametrized as $\Phi = (0, v+h)^T/\sqrt{2}$, so that the Goldstone modes are suppressed from the expansion. These degrees of freedom are hidden by the transformation to unitary gauge, and appear as the longitudinal parts of the $W^\pm$ and Z_0 bosons. With the covariant derivative from equation 2.2 we can insert the expansion of Φ into 2.1, to obtain

$$\begin{aligned}\mathcal{L}_{\text{Higgs}} &= \frac{1}{4}v^4\lambda + \frac{1}{2}(\partial_\mu h)(\partial^\mu h) - \frac{1}{2}m_h^2h^2 - \lambda v h^3 - \frac{1}{4}\lambda h^4 \\ &\quad + m_W^2 W_\mu^+ W^{\mu-} + m_W g W_\mu^+ W^{\mu-} h + \frac{1}{4}g^2 W_\mu^+ W^{\mu-} h^2 \\ &\quad + \frac{1}{2}m_Z^2 Z_\mu Z^\mu + \frac{m_Z g}{2\cos\theta_W} Z_\mu Z^\mu h + \frac{g^2}{8\cos^2\theta_W} Z_\mu Z^\mu h^2. \end{aligned} \tag{2.6}$$

Here we have identified the the Weinberg angle, $\cos\theta_W = g/\sqrt{g^2+g'^2}$, and the $W^\pm = (-W^1 \pm iW^2)/\sqrt{2}$ and $Z^0 = \cos\theta_W W_\mu^0 - \sin\theta_W B_\mu$ bosons, along with their masses $m_W = gv/2$ and $m_Z = \sqrt{g^2+g'^2}v/2 = gv/(2\cos\theta_W)$, respectively. Thus, we see that the masses of the $W^\pm$ and the Z_0 bosons derive from the vev v of the Higgs field.

We note that the Lagrangian 2.6 describes both cubic and quartic self-interactions of the Higgs field h. We will later consider such interactions as relevant phenomenological probes of BSM scenarios of the Higgs sector. For reference, we therefore note that the SM values of the cubic and quartic couplings, λ_{hhh} and λ_{hhhh}, respectively, can be extracted as follows

$$\lambda_{hhh} = \frac{3m_h^2}{v},\ \lambda_{hhhh} = \frac{3m_h^2}{v^2}, \tag{2.7}$$

with $m_h^2 = 2\lambda v^2$.

2.2 Elementary two-Higgs doublet models

A natural way to extend the Higgs sector of the SM is to add additional Higgs doublets. The most parsimonious such extension is the two-Higgs doublet model (2HDM), which

features two complex $SU(2)$ Higgs doublets Φ_1 and Φ_2. In this section we will describe the main features of elementary two-Higgs doublet models (E2HDM). Such models have been studied extensively; for reference, see the reviews [12, 13]. The scalar sector in 2HDM is given by

$$\mathcal{L}_{\rm 2HDM} = (D^\mu \Phi_1)^\dagger (D_\mu \Phi_1) + (D^\mu \Phi_2)^\dagger (D_\mu \Phi_2) - V_{\rm 2HDM}(\Phi_1, \Phi_2). \tag{2.8}$$

Here, the 2HDM potential $V_{\rm 2HDM}$ has the form

$$\begin{aligned} V_{\rm 2HDM} = {} & m_{11}^2 \Phi_1^\dagger \Phi_1 + m_{22}^2 \Phi_2^\dagger \Phi_2 - [m_{12}^2 \Phi_1^\dagger \Phi_2 + \text{ h.c.}] + \frac{1}{2}\lambda_1 (\Phi_1^\dagger \Phi_1)^2 \\ & + \frac{1}{2}\lambda_2 (\Phi_2^\dagger \Phi_2)^2 + \lambda_3 (\Phi_1^\dagger \Phi_1)(\Phi_2^\dagger \Phi_2) + \lambda_4 (\Phi_1^\dagger \Phi_2)(\Phi_2^\dagger \Phi_1) \\ & + \left[\frac{1}{2}\lambda_5 (\Phi_1^\dagger \Phi_2)^2 + [\lambda_6 (\Phi_1^\dagger \Phi_1) + \lambda_7 (\Phi_2^\dagger \Phi_2)](\Phi_1^\dagger \Phi_2) + \text{ h.c.} \right]. \end{aligned} \tag{2.9}$$

The reality of the potential requires that $m_{11}^2, m_{22}^2, \lambda_1, \lambda_2, \lambda_3$ and λ_4 are real. In general, $\lambda_5, \lambda_6, \lambda_7$ and m_{12}^2 may be complex. Unless a rephasing transformation can bring the potential to a form where all parameter values are real, complex values of $\lambda_5, \lambda_6, \lambda_7$ or m_{12}^2 induce $\mathcal{CP}$-violation [25]. We will not consider $\mathcal{CP}$-violating 2HDMs, and henceforth we will assume that all parameters of the Higgs potential are real. Further constraints apply to the potential parameters. For E2HDMs, we will only consider potentials which are bounded from below. Perturbativity and unitarity constraints also impose conditions on allowed values of the potential parameters, to be discussed below.

Like its SM counterpart, the 2HDM Higgs potential can have a nontrivial global minimum. This occurs if the mass matrix $[m_{ij}^2]$ is not positive definite. Charge and CP-conserving stationary points of the potential have the form

$$\langle \Phi_1 \rangle = \frac{1}{\sqrt{2}} \begin{pmatrix} 0 \\ v_1 \end{pmatrix} = \frac{v}{\sqrt{2}} \begin{pmatrix} 0 \\ c_\beta \end{pmatrix}, \langle \Phi_2 \rangle = \frac{1}{\sqrt{2}} \begin{pmatrix} 0 \\ v_2 \end{pmatrix} = \frac{v}{\sqrt{2}} \begin{pmatrix} 0 \\ s_\beta \end{pmatrix}, \tag{2.10}$$

where v_1 and v_2 denote the vev of Φ_1 and Φ_2 respectively, and where we introduced the basis angle β via $\tan\beta = v_2/v_1$. By a rephasing transformation $m_{12}^2 \to -m_{12}^2, \lambda_6 \to -\lambda_6, \lambda_7 \to -\lambda_7$ [25], one ensures that $\beta \in [0, \pi/2]$, following the convention in `2HDMC` [26].

By setting the first order derivatives of $V_{\rm 2HDM}$ with respect to v_1 and v_2 to zero, one obtains the following so-called tadpole conditions

$$\begin{cases} m_{11}^2 = m_{12}^2 t_\beta \ - \frac{1}{2} v^2 \left(\lambda_1 c_\beta^2 + \lambda_{345} s_\beta^2 + 3\lambda_6 s_\beta c_\beta + \lambda_7 s_\beta^2 t_\beta \right) \\ m_{22}^2 = m_{12}^2 t_\beta^{-1} - \frac{1}{2} v^2 \left(\lambda_2 s_\beta^2 + \lambda_{345} c_\beta^2 + \lambda_6 c_\beta^2 t_\beta^{-1} + 3\lambda_7 s_\beta c_\beta \right) \end{cases}, \tag{2.11}$$

with $s_\beta \equiv \sin\beta$, $c_\beta \equiv \cos\beta$, $t_\beta \equiv \tan\beta$ and $\lambda_{345} \equiv \lambda_3 + \lambda_4 + \lambda_5$.

Through the tadpole conditions, $V_{\rm 2HDM}$ is completely specified by the eight parameters m_{12}^2 and $\lambda_1, ..., \lambda_7$, for a given value of t_β and the vev v. While the vev v is a physical parameter, which in E2HDM will be fixed to the SM value $v = v_{\rm SM} = 246.22$ GeV, t_β is in general *not* a physical parameter, unless the 2HDM has special features that somehow

distinguish Φ_1 from Φ_2; so far, subindices 1 and 2 have just been arbitrary labels. As discussed in [27, 28], without such features, 2HDM observables must be invariant under a global Higgs-flavor $U(2)$ transformation of the form $\Phi_a \to \Phi'_a = U_{ab}\Phi_b$, where $U \in U(2)$. If the potential V_{2HDM} is written in terms of the transformed fields Φ'_a to have the same form as in equation 2.9, we see that the potential parameters also change, according to $m_{11}^2 \to (m_{11}^2)'$ etc., while t_β changes through equation 2.10. In this sense, β can be regarded as a basis angle, though its value does not uniquely determine the basis in terms of the Higgs-flavor $U(2)$ transformation [27]. When no restrictions are placed on the value of t_β, the basis is referred to as the general basis. An important choice of basis, that will be used below, where t_β *is* restricted, is the so-called Higgs basis, in which $\beta = 0$. In this basis, only Φ_1 gets a vev, i.e. $v_1 = v$ and $v_2 = 0$.

For a given minimum of the potential, we can expand the doublets around their respective vev in terms of the scalar fields $\varphi^\pm_{1,2}, \eta_{1,2}$ and $\chi_{1,2}$, according to [12]

$$\begin{cases} \Phi_1 = \dfrac{1}{\sqrt{2}}\begin{pmatrix} \sqrt{2}\varphi_1^+ \\ vc_\beta + \eta_1 + i\chi_1 \end{pmatrix} = \dfrac{1}{\sqrt{2}}\begin{pmatrix} \sqrt{2}(G^+c_\beta - H^+s_\beta) \\ vc_\beta - hs_\alpha + Hc_\alpha + i(G^0c_\beta - As_\beta) \end{pmatrix} \\ \Phi_2 = \dfrac{1}{\sqrt{2}}\begin{pmatrix} \sqrt{2}\varphi_2^+ \\ vs_\beta + \eta_2 + i\chi_2 \end{pmatrix} = \dfrac{1}{\sqrt{2}}\begin{pmatrix} \sqrt{2}(G^+s_\beta + H^+c_\beta) \\ vs_\beta + hc_\alpha + Hs_\alpha + i(G^0s_\beta + Ac_\beta) \end{pmatrix} \end{cases} \tag{2.12}$$

Here $G^0 = c_\beta\chi_1 + s_\beta\chi_2$ and $G^\pm = c_\beta\varphi_1^\pm + s_\beta\varphi_2^\pm$ denote the Goldstone bosons associated with the spontaneous symmetry breaking. The fields h, H, A and $H^\pm$ are massive Higgs bosons, where, by convention, $m_h \leq m_H$ and we identify h with the SM Higgs boson. The bosons h, H and A are all neutral, with h and H being CP-even, and A being CP-odd, whereas $H^\pm$ are charged. We have $H^\pm = -s_\beta\varphi_1^\pm + c_\beta\varphi_2^\pm$ and [2] $A = -s_\beta\chi_1 + c_\beta\chi_2$, while h and H are given by $h = -s_\alpha\eta_1 + c_\alpha\eta_2$ and $H = c_\alpha\eta_1 + s_\alpha\eta_2$. The angle α is a mixing angle that diagonalizes the mass matrix for the $\eta_{1,2}$ fields, to yield the mass eigenstates h and H; we assume the convention $\beta - \alpha \in [-\pi/2, \pi/2]$, consistent with `2HDMC` [26].

With these definitions in place and with the field expansion in 2.12, we can work out the masses. Explicitly, we have [29]

$$\begin{aligned} m_A^2 &= \frac{m_{12}^2}{s_\beta c_\beta} - \frac{1}{2}v^2(2\lambda_5 + \lambda_6 t_\beta^{-1} + \lambda_7 t_\beta) \\ m_{H^\pm}^2 &= m_A^2 + \frac{1}{2}v^2(\lambda_5 - \lambda_4) \end{aligned} \tag{2.13}$$

while the masses of h and H satisfy

$$\begin{pmatrix} m_H^2 & 0 \\ 0 & m_h^2 \end{pmatrix} = \mathcal{R}(\alpha)\mathcal{M}^2\mathcal{R}^T(\alpha), \quad \mathcal{R}(\alpha) = \begin{pmatrix} c_\alpha & s_\alpha \\ -s_\alpha & c_\alpha \end{pmatrix}, \tag{2.14}$$

[2] Assuming a $\mathcal{CP}$-conserving 2HDM.

where $\mathcal{M}^2$ denotes the mass matrix

$$\mathcal{M}^2 = m_A^2 \begin{pmatrix} s_\beta^2 & -s_\beta c_\beta \\ -s_\beta c_\beta & c_\beta^2 \end{pmatrix} + v^2 \begin{pmatrix} \lambda_1 c_\beta^2 + 2\lambda_6 s_\beta c_\beta + \lambda_5 s_\beta^2 & (\lambda_3+\lambda_4) s_\beta c_\beta + \lambda_6 c_\beta^2 \lambda_7 s_\beta^2 \\ (\lambda_3+\lambda_4) s_\beta c_\beta + \lambda_6 c_\beta^2 \lambda_7 s_\beta^2 & \lambda_2 s_\beta^2 + 2\lambda_7 s_\beta c_\beta + \lambda_5 c_\beta^2 \end{pmatrix}. \tag{2.15}$$

Let us now consider interactions in the 2HDM. First, we consider the interactions between vector bosons and Higgs bosons. The kinetic part of the Lagrangian is given by

$$\mathcal{L}_{\text{kin}} = (D^\mu \Phi_1)^\dagger (D_\mu \Phi_1) + (D^\mu \Phi_2)^\dagger (D_\mu \Phi_2), \tag{2.16}$$

with the gauge covariant derivative D_μ given by equation 2.2. Using the expansions in equation 2.12, the kinetic Lagrangian takes the form

$$\mathcal{L}_{\text{kin}} = \mathcal{L}_{\text{der}} + \mathcal{L}_{\text{mass}} + \mathcal{L}_{\text{VVH}} + \mathcal{L}_{\text{VHH}} + \mathcal{L}_{\text{VVHH}}, \tag{2.17}$$

where V generically stands for a vector boson and H for a Higgs field. The details are provided in appendix A.1. The corresponding trilinear couplings (VVH and VHH) are given in table 1 and the quartic couplings (VVHH) are given in table 2 . The operator $\overleftrightarrow{\partial}_\mu$ used in the expressions in these tables is defined by $X \overleftrightarrow{\partial}_\mu Y = X(\partial_\mu Y) - Y(\partial_\mu X)$. Note that the trilinear couplings for the $W_\mu^+ W^{\mu-} h$ and $Z_\mu Z^\mu h$ vertices are modified by the factor $\sin(\beta-\alpha)$ relative to the SM couplings, c.f. equation 2.6. In the so-called alignment limit $\beta - \alpha \to \pi/2$, we recover the SM values of these couplings.

Table 1: Trilinear couplings between gauge and Higgs bosons in the elementary 2HDM

Vertex	Coupling	Vertex	Coupling
$W_\mu^+ W^{\mu-} h$	$g m_W s_{\beta-\alpha}$	$W^{\mu-} H^+ \overleftrightarrow{\partial}_\mu H$	$-\frac{ig}{2} s_{\beta-\alpha}$
$W_\mu^+ W^{\mu-} H$	$g m_W c_{\beta-\alpha}$	$W^{\mu\pm} H^\mp \overleftrightarrow{\partial}_\mu A$	$\frac{g}{2}$
$Z_\mu Z^\mu h$	$\frac{g m_Z}{c_W} s_{\beta-\alpha}$	$Z^\mu A \overleftrightarrow{\partial}_\mu h$	$-\frac{g}{2c_W} c_{\beta-\alpha}$
$Z_\mu Z^\mu H$	$\frac{g m_Z}{c_W} c_{\beta-\alpha}$	$Z^\mu A \overleftrightarrow{\partial}_\mu H$	$\frac{g}{2c_W} s_{\beta-\alpha}$
$W^{\mu+} H^- \overleftrightarrow{\partial}_\mu h$	$-\frac{ig}{2} c_{\beta-\alpha}$	$Z^\mu H^- \overleftrightarrow{\partial}_\mu H^+$	$\frac{igc_{2W}}{2c_W}$
$W^{\mu-} H^+ \overleftrightarrow{\partial}_\mu h$	$\frac{ig}{2} c_{\beta-\alpha}$	$A^\mu H^- \overleftrightarrow{\partial}_\mu H^+$	ie
$W^{\mu+} H^- \overleftrightarrow{\partial}_\mu H$	$\frac{ig}{2} s_{\beta-\alpha}$		

Table 2: Quartic couplings between gauge and Higgs bosons in the elementary 2HDM

Vertex	Coupling	Vertex	Coupling
$W^+_\mu W^{\mu-} hh$	$\frac{g^2}{2}$	$Z_\mu Z^\mu H^+ H^-$	$\frac{g^2 c_{2W}^2}{2c_W^2}$
$W^+_\mu W^{\mu-} HH$	$\frac{g^2}{2}$	$W^\pm_\mu Z^\mu h H^\mp$	$\frac{g^2 s_W^2}{2c_W} c_{\beta-\alpha}$
$W^+_\mu W^{\mu-} AA$	$\frac{g^2}{2}$	$W^\pm_\mu Z^\mu H H^\mp$	$-\frac{g^2 s_W^2}{2c_W} s_{\beta-\alpha}$
$W^+_\mu W^{\mu-} H^+ H^-$	$\frac{g^2}{4}$	$W^\pm_\mu A^\mu h H^\mp$	$-\frac{ge}{2} c_{\beta-\alpha}$
$Z_\mu Z^\mu hh$	$\frac{g^2}{2c_W^2}$	$W^\pm_\mu A^\mu H H^\mp$	$\frac{ge}{2} s_{\beta-\alpha}$
$Z_\mu A^\mu H^+ H^-$	$Z_\mu Z^\mu HH$	$\frac{g^2}{2c_W^2}$	$\frac{gec_{2W}}{c_W}$
$Z_\mu Z^\mu AA$	$\frac{g^2}{2c_W^2}$	$A_\mu A^\mu H^+ H^-$	$2e^2$

Next, we consider the Higgs self interactions, which are obtained by substituting the field expansions in equation 2.12 into the 2HDM potential V_{2HDM} in equation 2.9. If we label the Higgs fields by $(h_1, h_2, h_3, h_4, h_5) = (h, H, A, H^+, H^-)$ the cubic and quartic Higgs self couplings, $\lambda_{h_i h_j h_k}$ and $\lambda_{h_i h_j h_k h_l}$ respectively, are given by

$$\lambda_{h_i h_j h_k} = \frac{\partial^3 V_{\text{2HDM}}}{\partial h_i \partial h_j \partial h_k}, \quad \lambda_{h_i h_j h_k h_l} = \frac{\partial^4 V_{\text{2HDM}}}{\partial h_i \partial h_j \partial h_k \partial h_l}. \tag{2.18}$$

We will not list all the self couplings here, but focus on those which are most relevant phenomenologically. Expressions for all the couplings can be found in e.g. [28]. The self couplings are most easily expressed in the Higgs basis, where the basis angle $\beta = 0$. The quartic couplings in the Higgs basis corresponding to $\lambda_1, ..., \lambda_7$ are denoted by $\Lambda_1, ..., \Lambda_7$. The relationship between these parameters can be found in e.g. [28]. The Higgs self couplings that we will focus on are given in table 3 below. We write the vev as v_{SM} in table 3, for later comparison to the composite case.

Table 3: Selected Higgs self couplings in the elementary 2HDM

Vertex	Coupling
hhh	$-3v_{\text{SM}}\left[(3\Lambda_6 - \Lambda_7)c^3_{\beta-\alpha} + (\Lambda_1 - \Lambda_{345})c^2_{\beta-\alpha}s_{\beta-\alpha} - 3\Lambda_6 c_{\beta-\alpha} - \Lambda_1 s_{\beta-\alpha}\right]$
hhH	$-v_{\text{SM}}\left[3(\Lambda_1 - \Lambda_{345})c^3_{\beta-\alpha} - 3(3\Lambda_6 - \Lambda_7)c^2_{\beta-\alpha} - (3\Lambda_1 - 2\Lambda_{345})c_{\beta-\alpha} + 3\Lambda_6 s_{\beta-\alpha}\right]$
hHH	$v_{\text{SM}}\left[3(3\Lambda_6 - \Lambda_7)c^3_{\beta-\alpha} + 3(\Lambda_1 - \Lambda_{345})c^2_{\beta-\alpha}s_{\beta-\alpha} - 3(2\Lambda_6 - \Lambda_7)c_{\beta-\alpha} + \Lambda_{345}s_{\beta-\alpha}\right]$
hAA	$v_{\text{SM}}\left[\Lambda_7 c_{\beta-\alpha} + (\Lambda_3 + \Lambda_4 - \Lambda_5)s_{\beta-\alpha}\right]$
hH^+H^-	$v_{\text{SM}}\left[\Lambda_7 c_{\beta-\alpha} + \Lambda_3 s_{\beta-\alpha}\right]$
$hhhh$	$3(\Lambda_1 + \Lambda_2 - 2\Lambda_{345})c^4_{\beta-\alpha} - 12(\Lambda_6 - \Lambda_7)c^3_{\beta-\alpha}s_{\beta-\alpha} - 6(\Lambda_1 - \Lambda_{345})c^2_{\beta-\alpha}$ $+12\Lambda_6 c_{\beta-\alpha}s_{\beta-\alpha} + 3\Lambda_1$

Finally, we consider the fermionic sector. The general expression for the Yukawa Lagrangian can be found in [28], and is given by

$$\begin{aligned}
-\mathcal{L}_{\text{Yukawa}} = &\frac{1}{\sqrt{2}}\bar{D}\{\kappa^D s_{\beta-\alpha} + \rho^D c_{\beta-\alpha}\}Dh + \frac{1}{\sqrt{2}}\bar{D}\{\kappa^D s_{\beta-\alpha} - \rho^D c_{\beta-\alpha}\}DH + \frac{i}{\sqrt{2}}\bar{D}\gamma_5\rho^D DA \\
&+ \frac{1}{\sqrt{2}}\bar{U}\{\kappa^U s_{\beta-\alpha} + \rho^U c_{\beta-\alpha}\}Uh + \frac{1}{\sqrt{2}}\bar{U}\{\kappa^U s_{\beta-\alpha} - \rho^U c_{\beta-\alpha}\}UH - \frac{i}{\sqrt{2}}\bar{U}\gamma_5\rho^U UA \\
&+ \frac{1}{\sqrt{2}}\bar{L}\{\kappa^L s_{\beta-\alpha} + \rho^L c_{\beta-\alpha}\}Lh + \frac{1}{\sqrt{2}}\bar{L}\{\kappa^L s_{\beta-\alpha} - \rho^L c_{\beta-\alpha}\}LH + \frac{i}{\sqrt{2}}\bar{L}\gamma_5\rho^L LA \\
&+ [\bar{U}\{V_{\text{CKM}}\rho^D P_R - \rho^U V_{\text{CKM}} P_L\}DH^+ + \bar{\nu}\rho^L P_R LH^+ + \text{h.c.}]. \qquad (2.19)
\end{aligned}$$

Here $U = (u, c, t)^T$, $D = (d, s, b)^T$, $L = (e, \mu, \tau)^T$ and $\nu = (\nu_e, \nu_\mu, \nu_\tau)^T$ are fermion vectors in flavor space for up-type quarks, down-type quarks, leptons and neutrinos, respectively. The matrices κ^F are defined by $\kappa^F = \sqrt{2}M^F/v$, where M^F denotes the diagonal mass matrix for the fermions ($F = U, D, L$) [3]. The matrices ρ^F are, in principle, general matrices, though in a $\mathcal{CP}$-conserving model, they must be symmetric [28]. In order to limit flavor-changing neutral currents (FCNCs) at tree-level, the off-diagonal elements of the ρ^F matrices cannot be large. We will only consider the 2HDM with flavor alignment, i.e. where the fermionic mass matrices and flavor matrices can be simultaneously diagonalized, which guarantees the FCNCs are not present at tree-level. Under this assumption, the ρ^F matrices are diagonal, and we will henceforth use ρ_f to denote the diagonal element of the appropriate ρ^F matrix for the fermion flavor f; in a similar spirit, we use κ_f to denote the diagonal element of the appropriate κ^F matrix. Finally, in equation 2.19 V_{CKM} denotes the CKM matrix, and $P_{R/L}$ denote the projection operators $P_{R/L} = (1 \pm \gamma_5)/2$.

2.3 Composite two-Higgs doublet models

In composite Higgs models (CHMs) [17], the Higgs boson (or bosons, in multi-Higgs models) is, unlike in the SM, not an elementary state but rather a composite state of a new strong interaction, with an associated global symmetry group $\mathcal{G}$. Specifically, the Higgs boson is interpreted as a composite state of a set of new (heavy) fermions associated with the new strong interaction. Such a setup is similar to how the mesons of the SM are composite states of SM fermions, governed by QCD.

In this construction, the Higgs boson arises as a Goldstone boson by the spontaneous symmetry breaking [4] of $\mathcal{G}$ down to some subgroup $\mathcal{H}$, with an associated compositeness energy scale f; in the orignal CHM [17], this breaking pattern is $SU(5) \to SO(5)$. If the global symmetry were exact and the Higgs were truly a Goldstone boson, it would be massless. Therefore some form of explicit symmetry breaking, to be specified below, must be present, in order to give mass to the Higgs boson; the Higgs boson is then realized as a *pseudo* Goldstone boson (pGB). In this sense, returning to the QCD analogy, the Higgs

[3] We assume neutrinos to be massless.

[4] Recall Goldstone's theorem [24] as discussed in section 2.1: When a global symmetry is spontaneously broken, there arises a massless Goldstone boson for each broken generator

boson would be similar to pions. Indeed, these are composites of SM fermions and can be regarded as pGBs associated with chiral symmetry breaking in QCD, with the explicit symmetry breaking provided by the nonzero quark masses. Since the mass of the Higgs boson, if realized as a pGB in a CHM, is naturally kept lower than the compositeness scale f, CHMs can solve the fine tuning problem, as discussed in the introduction.

In this thesis, we are interested in composite 2HDMs (C2HDMs), which are treated in [18]. As discussed in [18], C2HDMs can be realized by different spontaneous symmetry breaking patterns $\mathcal{G} \to \mathcal{H}$, but there are phenomenological constraints that restrict the breaking patterns which would give rise to models that can be matched to available collider phenomenology. Specifically, the oblique T-parameter [30], to be further discussed in section 3.3.2, must be kept small, by ensuring that the subgroup $\mathcal{H}$ has a so-called custodial $SO(4)$ symmetry. One breaking pattern allowed by this requirement is $SO(6) \to SO(4) \times SO(2)$, which provides $6 \times 5/2 - (4 \times 3/2 + 2 \times 1/2) = 8$ (pseudo) Goldstone bosons which can be identified with the eight Higgs fields in 2HDMs. The explicit breaking of $\mathcal{G}$ will be realized through the so-called partial compositeness paradigm [31], by interactions between the elementary fields and the fields (resonances) of the new strong sector.

This brief introduction provides the background for the particular C2HDM considered in [19]. We will not provide a full description of all aspects of the model, but try to capture the most important features. The group structure is based on the pattern $SO(6) \to SO(4) \times SO(2)$ discussed above, and is given by

$$\frac{\mathcal{G}}{\mathcal{H}} = \frac{SU(3)_C \times SO(6) \times U(1)_X}{SU(3)_C \times SO(4) \times SO(2) \times U(1)_X}, \tag{2.20}$$

where $U(1)_X$ is a gauge group. As discussed above, the explicit symmetry breaking is realized through the partial compositeness paradigm, with a strong sector governed by $SO(6) \times U(1)_X$ and an elementary sector governed by $SO(6) \times U(1)_X$, containing the SM electroweak gauge group $SU(2)_L \times U(1)_Y$ as a subgroup. Aside from the pGBs, realized from the spontaneous breaking of $SO(6) \times U(1)_X \to SO(4) \times SO(2) \times U(1)_X$ and identified with the eight Higgs fields, and the elementary SM fields, the model contains spin-1 and spin-1/2 resonances associated with the strong sector.

As already mentioned, the eight pGBs associated with $SO(6) \to SO(4) \times SO(2)$ breaking can be associated with the eight scalar fields in 2HDM. The associated Higgs potential has been calculated in [19] according to the Coleman-Weinberg [32] mechanism, and is given at one-loop order by

$$iV_{\text{C2HDM}} = \frac{1}{f^4} \int \frac{d^4k}{(2\pi)^4} \left[\frac{3}{2} V_G(\Phi_1, \Phi_2) - 6V_F(\Phi_1, \Phi_2) \right] + \mathcal{O}\left(\frac{1}{f^4}\right). \tag{2.21}$$

In this equation, $V_G(\Phi_1, \Phi_2)$ and $V_F(\Phi_1, \Phi_2)$ are potentials with the same form as the 2HDM potential in equation 2.9, and associated with the gauge and fermion sectors, respectively.

Taking only the leading contributions into account, from the top-quark spin-1/2 resonances and the spin-1 gauge resonances into account, the potential is defined by the following parameters: f, g_ρ, Y_1^{12}, Y_2^{12}, Δ_L^1, Δ_R^2, M_Ψ^{11}, M_Ψ^{22} and M_Ψ^{12}. Here, f is the compositeness scale, g_ρ the gauge coupling, Δ_L^1 and Δ_R^2 are mixing parameters between the

elementary and strong sectors, Y_1^{12} and Y_2^{12} are Yukawa couplings for the top resonances, and M_Ψ^{11}, M_Ψ^{22} and M_Ψ^{12} are mass parameters of the top resonances. The associated potential parameters are then given by

$$m_{ij}^2 = \frac{-i}{f^4}\int \frac{d^4k}{(2\pi)^4}\left[\frac{3}{2}(m_{ij}^G)^2 - 6(m_{ij}^F)^2\right],\ \lambda_i = \frac{-i}{f^4}\int \frac{d^4k}{(2\pi)^4}\left[\frac{3}{2}\lambda_i^G - 6\lambda_i^F\right]. \tag{2.22}$$

These can be calculated from the expression provided in [19]. We provide some further details on this in appendix B.2. Note, in particular, that $\lambda_6 = \lambda_7$ and that $\lambda_6 = \lambda_7 = (5/3)m_{12}^2$.

Let us now discuss the phenomenology of the model. As already mentioned, there are various phenomenological consequences of the new dynamics in the composite 2HDM model, both compared to the case of an elementary 2HDM, but also, of course, compared to the SM. As we have just seen, in the composite case, the potential parameters are calculated from the underlying parameters of the composite model, which introduces correlations, that are not present in the elementary case, between masses and couplings. The couplings also get modified relative to their values in the elementary case, which we will now discuss.

One source of these modifications derives from the vev of the Higgs doublets in the composite model. From the gauge sector Lagrangian, the following relation can be derived [19]

$$v_{\text{SM}}^2 = f^2 \sin^2\frac{v}{f}, \tag{2.23}$$

by demanding that the masses of the $W^\pm$ and Z^0 bosons satisfy $m_W = g v_{\text{SM}}/2$ and $m_Z = m_W/\cos\theta_W$ (see the paragraph below equation 2.6). Equation 2.23 relates the vev v_{SM} of the SM (which we also take to be the vev of the elementary 2HDM) to the vev $v = \sqrt{v_1^2 + v_2^2}$, with $v_{1,2}$ being the vevs of the two Higgs doublets. Equation 2.23 says that for a given f and v, the SM vev is determined by equation 2.23. When implementing the composite 2HDM, as discussed in section 3.5, we will require that the value $v_{\text{SM}}^{\text{calc}}$ calculated from equation 2.23 should agree with 246.22 GeV within a narrow range, taken to be 2%. In this context, let us introduce the parameter ξ given by

$$\xi = \frac{v_{\text{SM}}^2}{f^2}, \tag{2.24}$$

which we will use to parametrize the deviations to various couplings in the composite 2HDM compared to the elementary 2HDM. By Taylor expansion of equation 2.23, we obtain the approximate relationship

$$v = v_{\text{SM}}\left(1 + \frac{\xi}{6} + \mathcal{O}(\xi^2)\right), \tag{2.25}$$

which is used to relate v to v_{SM} at first order in ξ.

Further modifications to the couplings derive from the rescaling of the Higgs fields, to make them canonically normalized [33]. In the Higgs basis, the two-derivative Lagrangian

of the field η_2, which appears in the expansion of the Higgs doublets in equation 2.12, is given by

$$\mathcal{L}_{2-\mathrm{der},\eta_2} = \frac{1}{2}\left(1 - \frac{1}{3}\xi + \mathcal{O}(\xi^2)\right)(\partial_\mu \eta_2)(\partial^\mu \eta_2). \tag{2.26}$$

In order to make η_2 canonically normalized, so that the mass eigenstates in the composite model can be compared to those in the elementary case, the field has to be rescaled according to

$$\eta_2 \to \left(1 - \frac{\xi}{3}\right)^{-1/2} \eta_2 = \left(1 + \frac{\xi}{6} + \mathcal{O}(\xi^2)\right)\eta_2. \tag{2.27}$$

The total modifications have been calculated in [19], and we give the most important ones here for reference. The trilinear couplings between gauge and Higgs bosons are given in table 4 (c.f. table 1 for the elementary 2HDM). We do not give the full expressions for the self couplings here, since they are quite lengthy. For example, the modified λ_{hhh} is given by

$$\begin{aligned}\lambda_{hhh} =& -3v_{\mathrm{SM}}\left[(3\Lambda_6 - \Lambda_7)c_{\beta-\alpha}^3 + (\Lambda_1 - \Lambda_{345})c_{\beta-\alpha}^2 s_{\beta-\alpha} - 3\Lambda_6 c_{\beta-\alpha} - \Lambda_1 s_{\beta-\alpha}\right] \\ & -3\xi v_{\mathrm{SM}}\left[\left(\Lambda_6 - \frac{2}{3}\Lambda_7\right)c_{\beta-\alpha}^3 + \frac{1}{6}(\Lambda_1 - \Lambda_{345})c_{\beta-\alpha}^2 s_{\beta-\alpha} - \Lambda_6 c_{\beta-\alpha} - \frac{1}{6}\Lambda_1 s_{\beta-\alpha}\right]\end{aligned} \tag{2.28}$$

Table 4: Trilinear couplings between gauge and Higgs bosons in C2HDM [19].

Vertex	Coupling	Vertex	Coupling
$W_\mu^+ W^{\mu-} h$	$g m_W (1-\xi/2) s_{\beta-\alpha}$	$W^{\mu-} H^+ \overleftrightarrow{\partial}_\mu H$	$-\frac{ig}{2} s_{\beta-\alpha}$
$W_\mu^+ W^{\mu-} H$	$g m_W (1-\xi/2) c_{\beta-\alpha}$	$W^{\mu\pm} H^\mp \overleftrightarrow{\partial}_\mu A$	$\frac{g}{2}$
$Z_\mu Z^\mu h$	$\frac{g m_Z}{c_W}(1-\xi/2) s_{\beta-\alpha}$	$Z^\mu A \overleftrightarrow{\partial}_\mu h$	$-\frac{g}{2c_W} c_{\beta-\alpha}$
$Z_\mu Z^\mu H$	$\frac{g m_Z}{c_W}(1-\xi/2) c_{\beta-\alpha}$	$Z^\mu A \overleftrightarrow{\partial}_\mu H$	$\frac{g}{2c_W} s_{\beta-\alpha}$
$W^{\mu\pm} H^\mp \partial_\mu h$	$\mp\frac{ig}{2}(1-5\xi/6) c_{\beta-\alpha}$	$Z^\mu H^- \overleftrightarrow{\partial}_\mu H^+$	$\frac{igc_{2W}}{2c_W}$
$W^{\mu\pm} h \partial_\mu H^\mp$	$\pm\frac{ig}{2}(1-\xi/6) c_{\beta-\alpha}$	$Z^\mu H^- \overleftrightarrow{\partial}_\mu H^+$	$\frac{igc_{2W}}{2c_W}$
$W^{\mu-} H^+ \overleftrightarrow{\partial}_\mu h$	$\frac{ig}{2} c_{\beta-\alpha}$	$A^\mu H^- \overleftrightarrow{\partial}_\mu H^+$	ie
$W^{\mu+} H^- \overleftrightarrow{\partial}_\mu H$	$\frac{ig}{2} s_{\beta-\alpha}$		

Finally, the fermionic interactions in C2HDM are governed by a flavour aligned Yukawa Lagrangian, given by [19]

$$
\begin{aligned}
-\mathcal{L}_{\text{Yukawa}} = &\sum_f \frac{m_f}{v_{\text{SM}}} \left[\xi_h^f h + \xi_H^f H - 2iI_f \xi_A^f A\gamma^5\right] f \\
&+ \frac{\sqrt{2}}{v_{\text{SM}}} \left[V_{ud}\bar{u}\left(-\xi_A^u m_u P_L + \xi_A^d m_d P_R\right) dH^+ + \xi_A^l m_l \bar{\nu} P_R l H^+ + \text{h.c.}\right],
\end{aligned} \tag{2.29}
$$

where $I_f = 1/2(-1/2)$ for $f = u(d,l)$ and where we introduced the coefficients

$$
\begin{aligned}
\xi_h^f &= (1 + c_h^f \xi) s_{\beta-\alpha} - (\zeta_f + c_h^f \xi) c_{\beta-\alpha} \\
\xi_H^f &= (1 + c_h^f \xi) c_{\beta-\alpha} + (\zeta_f + c_h^f \xi) s_{\beta-\alpha}, \\
\xi_A^f &= \zeta_f + c_A^f
\end{aligned} \tag{2.30}
$$

with

$$
\begin{aligned}
&c_h^f = -\frac{1}{2}\frac{3 + \bar{\zeta}_f t_\beta}{1 + \bar{\zeta}_f t_\beta}, \quad c_H^f = \frac{1}{2}\frac{\bar{\zeta}_f (1 + t_\beta^2)}{(1 + \bar{\zeta}_f t_\beta)^2}, \quad c_A^f = -\frac{1}{2}\frac{t_\beta (1 + \bar{\zeta}_f)^2}{(1 + \bar{\zeta}_f t_\beta)^2} \\
&\zeta_f = \frac{\bar{\zeta}_f - t_\beta}{1 + \bar{\zeta}_f t_\beta}, \quad \bar{\zeta}_f = -\frac{Y_1^f}{Y_2^f}
\end{aligned} . \tag{2.31}
$$

Note, then, that in C2HDM, the structure of the Yukawa Lagrangian differs at $\mathcal{O}(\xi)$ from the elementary case, c.f. equation 2.50. Formally, we can make the following translations of κ_f and ρ_f:

$$
\begin{aligned}
h, H : \kappa_f &= \frac{\sqrt{2} m_f}{v_{\text{SM}}}(1 + c_h^f \xi), \quad \rho_f = -\frac{\sqrt{2} m_f}{v_{\text{SM}}}(\zeta_f + c_f^h \xi) \\
A, H^\pm : \rho_f &= \frac{\sqrt{2} m_f}{v_{\text{SM}}}(\zeta_f + c_A^f \xi)
\end{aligned} \tag{2.32}
$$

2.4 Phase transitions

2.4.1 The effective potential

A phase transition is associated with the change in the ground state configuration of a system as the temperature passes a critical value. To study this phenomenon, we must consider the temperature dependent potential at finite temperature [5]. At tree-level, the potential, such as in equations 2.3 or 2.9, has no temperature dependence, so this dependence necessarily enters as a loop effect. Consider a system with a set of n_S scalar fields $\phi_1, ..., \phi_{n_S}$, that we write collectively in vector notation as $\boldsymbol{\phi} = (\phi_1, ..., \phi_{n_S})$, and with the tree-level potential V_{tree}. Let $\boldsymbol{\omega} = (w_1, ..., w_{n_S})$ denote the ground state configuration (vacuum). Then the one-loop corrected potential $V_1(\boldsymbol{\phi})$ at zero temperature has the form

$$
V_1(\boldsymbol{\phi}) = V_{\text{tree}}(\boldsymbol{\phi}) + V_{\text{CW}}(\boldsymbol{\phi}) + V_{\text{CT}}(\boldsymbol{\phi}), \tag{2.33}
$$

[5] In standard physics jargon, this refers to non-zero temperature, i.e. finite inverse temperature.

where V_{CW} is the Coleman-Weinberg potential [32] and V_{CT} is the counterterm potential. Here we write the argument of the potential as $\boldsymbol{\phi}$, but we emphasize that aside from when we consider the counterterms in equation 2.35, the potential will be evaluated at the background field $\boldsymbol{\omega}$.

The Coleman-Weinberg potential is the one-loop correction to the tree-level potential, and is given by

$$V_{\text{CW}}(\boldsymbol{\phi}) = \sum_i \pm \frac{n_i}{64\pi^2} m_i^4(\boldsymbol{\phi}) \left(\ln \left[\frac{m_i^2(\boldsymbol{\phi})}{Q^2} \right] - c_i \right), \tag{2.34}$$

where the sum runs over all fields in the theory and + applies for bosons, while − applies for fermions. Note that the summation includes the Goldstone modes and the photon modes, and that transverse (T) and longitudinal (L) modes are counted separately. The parameter n_i denotes the number of degrees of freedom of field i, and will be specified later when we consider concrete models. Further, the coefficient c_j is determined by the renormalization scheme for the Coleman-Weinberg potential; in the modified minimal subtraction ($\overline{\text{MS}}$) scheme, c_j is given by $c_j = 1/2$ for transverse gauge boson polarizations and $c_j = 3/2$ for all other fields (fermions and longitudinal gauge boson polarizations). The renormalization scale is denoted by Q, and will be set to the SM vev throughout, i.e. $Q = 246.22$ GeV. Finally, $m_i^2(\boldsymbol{\phi})$ denotes the squared field dependent tree-level mass (at zero temperature) of field i. The field dependent masses $m_i^2(\boldsymbol{\phi})$ are determined by diagonalization of the Hessian H of V_{tree}, with components $H_{ij} = (1/2)\partial^2 V_{\text{tree}}(\boldsymbol{\phi})/\partial\phi_i\partial\phi_j$. We emphasize that aside from when we consider the counterterms in equation 2.35 below, the field dependent masses are evaluated at $\boldsymbol{\omega}$, and are determined by the diagonalization of the Hessian with components $H_{ij} = (1/2)\partial^2 V_{\text{tree}}(\boldsymbol{\phi})/\partial\phi_i\partial\phi_j|_{\boldsymbol{\phi}=\boldsymbol{\omega}}$.

The additional counterterm potential V_{CT} has the same form as V_{tree}, and may be introduced to enforce certain conditions on the loop-corrected potential V_1. A reasonable requirement is that the loop corrected potential $V_{\text{tree}} + V_{\text{CW}} + V_{\text{CT}}$ (without the thermal corrections) has the same minimum and the same masses at the minimum as V_{tree}, as done e.g. in [34]. If we let $\boldsymbol{v}$ denote the ground state configuration of V_{tree}, these conditions can be written as

$$\begin{cases} \left.\dfrac{\partial V_{\text{CT}}(\boldsymbol{\phi})}{\partial\phi_i}\right|_{\boldsymbol{\phi}=\boldsymbol{v}} = -\left.\dfrac{\partial V_{\text{CW}}(\boldsymbol{\phi})}{\partial\phi_i}\right|_{\boldsymbol{\phi}=\boldsymbol{v}}, \ i = 1, ..., n_S \\ \left.\dfrac{\partial^2 V_{\text{CT}}(\boldsymbol{\phi})}{\partial\phi_i\phi_j}\right|_{\boldsymbol{\phi}=\boldsymbol{v}} = -\left.\dfrac{\partial^2 V_{\text{CW}}(\boldsymbol{\phi})}{\partial\phi_i\partial\phi_j}\right|_{\boldsymbol{\phi}=\boldsymbol{v}}, \ i, j = 1, ..., n_S \end{cases} \tag{2.35}$$

From equation 2.34, we see immediately that the second counterterm condition may be problematic for the Goldstone modes in the Coleman-Weinberg potential. Indeed the second derivatives of V_{CW} will involve terms of the form $(\partial m_k^2(\boldsymbol{\phi})/\partial\phi_i)(\partial m_k^2(\boldsymbol{\phi})/\partial\phi_j)\times$ $\ln[m_k^2(\boldsymbol{\phi})/Q^2]$, which may diverge when evaluated at $\boldsymbol{\phi} = \boldsymbol{v}$ for a Goldstone mode, since these have $m_k^2(\boldsymbol{v}) = 0$. This may be addressed by simply removing the Goldstone modes from the summation altogether in V_{CW}, as done in e.g. [35]. In [36], it is instead argued that the Goldstone modes should be included in the summation, but that when evaluating terms of the form $(\partial m_k^2(\boldsymbol{\phi})/\partial\phi_i)(\partial m_k^2(\boldsymbol{\phi})/\partial\phi_j)\ln[m_k^2(\boldsymbol{\phi})/Q^2]$ for a Goldstone mode at $\boldsymbol{\phi} = \boldsymbol{v}$,

one should replace $m_k^2(\boldsymbol{\phi})|_{\boldsymbol{\phi}=\boldsymbol{v}} = 0$ by some nonzero cutoff value. We mention these issues to highlight that it is not straightforward to correctly implement the counterterms. In practice, in our investigations of 2HDMs, we will use a greatly simplified counterterm potential on which we only impose the first counterterm condition in 2.35; see equations 2.52 and 2.53.

Above, we introduced the field dependent masses at zero temperature. At finite temperature, the masses (aside from those corresponding to transverse polarization modes of the gauge bosons) receive corrections of order T^2 [37, 38]; hence we introduce the notation $m_i^2(\boldsymbol{\omega}, T)$ for the field and temperature dependent mass of field i. These masses are given by diagonalization of the matrix $H + \Pi$, where Π represents the leading order temperature corrections. Explicit expression will be given later when we consider concrete models. The origin of these temperature dependent corrections is the breakdown of the perturbative expansion in terms of the couplings in V_{tree} at high temperature. A resummation has to be performed (called a daisy resummation), which effectively leads to the addition of the one-loop polarization tensor Π to the mass matrix [37, 38].

There are different ways in which these temperature dependent masses can be accommodated. In the "Arnold-Espinosa method" (AE) [34, 39, 38], the thermal corrections to the masses do not enter V_{CW} or V_{CT}. The one loop corrected thermal *effective* potential $V_{\text{eff}}^{\text{AE}}(\boldsymbol{\phi}, T)$ at temperature T is then given by

$$V_{\text{eff}}^{\text{AE}}(\boldsymbol{\omega}, T) = V_{\text{tree}}(\boldsymbol{\omega}) + V_{\text{CW}}(\boldsymbol{\omega}) + V_{\text{CT}}(\boldsymbol{\omega}) + \Delta V_T(\boldsymbol{\omega}, T) + V_{\text{daisy}}(\boldsymbol{\omega}, T). \tag{2.36}$$

Here ΔV_T is a thermal correction term, which is given by [38]

$$\Delta V_T(\boldsymbol{\omega}, T) = \sum_i \pm \frac{n_i}{2\pi^2} T^4 J_\pm \left(m_i^2(\boldsymbol{\omega})/T^2 \right). \tag{2.37}$$

Again, $+$ applies for bosons while $-$ applies for fermions, and the integrals $J_\pm$ are given by

$$J_\pm(x^2) = \int_0^\infty \xi^2 \ln \left[1 \mp \exp(-\sqrt{x^2 + \xi^2}) \right] d\xi. \tag{2.38}$$

For small x^2, corresponding to the high temperature limit, we have the following expansion that we will need later on: [34, 38]

$$\begin{cases} J_+(x^2) = -\dfrac{\pi^4}{45} + \dfrac{\pi^2}{12} x^2 - \dfrac{\pi}{6} x^3 - \dfrac{1}{32} x^4 \left(\ln x^2 - \ln a_b \right) + \mathcal{O}(x^6) \\ J_-(x^2) = \dfrac{7\pi^4}{360} - \dfrac{\pi^2}{24} x^2 - \dfrac{1}{32} x^4 \left(\ln x^2 - \ln a_f \right) + \mathcal{O}(x^6) \end{cases} \tag{2.39}$$

where $\ln a_b = 2\ln\pi + 4\ln 2 + \frac{3}{2} - 2\gamma_E \approx 5.4076$ and $\ln a_f = 2\ln\pi + \frac{3}{2} - 2\gamma_E \approx 2.6351$, with $\gamma_E \approx 0.57722$ denoting the Euler-Mascheroni constant.

Meanwhile, the second term $V_{\text{daisy}}(\boldsymbol{\omega}, T)$ in equation 2.36 is given by

$$V_{\text{daisy}}(\boldsymbol{\omega}, T) = -\frac{T}{12\pi} \sum_{i,\text{bosons}} n_i \left(\left[m_i^2(\boldsymbol{\omega}, T) \right]^{3/2} - \left[m_i^2(\boldsymbol{\omega}) \right]^{3/2} \right). \tag{2.40}$$

Note that the addition of $V_{\text{daisy}}(\boldsymbol{\omega}, T)$ means that in the sum $\Delta V_T(\boldsymbol{\omega}, T) + V_{\text{daisy}}(\boldsymbol{\omega}, T)$, the temperature dependent masses $m_i^2(\boldsymbol{\omega}, T)$ effectively appear in the cubic term only in the thermal integral J_+ (see equation 2.39).

Let us comment on the physical meaning of the terms ΔV_T. By construction, the term ΔV_T corresponds to the difference between the one-loop effective potential at finite temperature and the one-loop effective potential at zero temperature. However, it can also be given a very direct physical interpretation as the total free energy contribution from each individual particle species in the ideal gas approximation [40]. That is,

$$\Delta V_T(\boldsymbol{\omega}, T) = \sum_i f_i(\boldsymbol{\omega}, T) = -\sum_i p_i(\boldsymbol{\omega}, T) \tag{2.41}$$

where $f_i = -p_i$ denotes the free energy contribution from particle species i, with p_i denoting the corresponding pressure.

In the "Parwani method" (P) [41, 34], on the other hand, there is no term V_{daisy} in V_{eff}. Meanwhile the temperature dependent masses $m_j^2(\boldsymbol{\phi}, T)$ are used in V_{CW} and in ΔV_T. If we introduce the notations $V_{\text{CW}}^{\text{P}}(\boldsymbol{\omega}, T)$ and $\Delta V_T^{\text{P}}(\boldsymbol{\omega}, T)$ for the Coleman-Weinberg and thermal correction potential, respectively, with the replacement $m_i^2(\boldsymbol{\omega}) \to m_i^2(\boldsymbol{\omega}, T)$ made, the effective potential $V_{\text{eff}}^{\text{P}}(\boldsymbol{\phi}, T)$ is given by

$$V_{\text{eff}}^{\text{P}}(\boldsymbol{\omega}, T) = V_{\text{tree}}(\boldsymbol{\omega}) + V_{\text{CW}}^{\text{P}}(\boldsymbol{\omega}, T) + V_{\text{CT}}(\boldsymbol{\omega}) + \Delta V_T^{\text{P}}(\boldsymbol{\omega}, T). \tag{2.42}$$

Note that even though V_{CW}^{P} depends on the temperature through the $m_i^2(\boldsymbol{\omega}, T)$, V_{CT} is not temperature dependent, since the counterterm conditions in equation 2.35 are imposed at $T = 0$. The physical interpretation of the different terms is similar to the interpretation in the Arnold-Espinosa method, and we will not elaborate further on the differences. We will use the Parwani method throughout, since this is the method which is implemented in the `CosmoTransitions` package [42], to be described later.

A furher issue, aside from the question of how to correctly implement the temperature corrections to the field dependent masses, has to do with gauge dependence of the effective potential and the observables derived from it. The equations above are given in so-called Landau gauge, which corresponds to the limit $\xi \to 0$ for the gauge parameter ξ. Care is required to make sure that observables are calculated in a way that gives gauge invariant results. For a recent discussion about these issues and how to resolve them, see [43]. We will not consider these issues, and note that doing so introduces an uncertainty to our calculations.

2.4.2 Phase transitions in the SM

To be more concrete, let us now consider phase transitions in (a simplified version of) the SM. If we neglect the temperature corrections to the masses and only take the $W^{\pm}$ and Z^0 bosons, as well as the top quark into account for the loop corrections, we obtain, in the high temperature expansion of equation 2.39, an effective potential at finite temperature given by [38]

$$V_{\text{eff}}(\omega, T) = D(T^2 - T_0^2)\omega^2 - ET\omega^3 + \frac{1}{4}\lambda(T)\omega^4, \tag{2.43}$$

where

$$D = \frac{2m_W^2 + m_Z^2 + 2m_t^2}{8v^2},\ E = \frac{2m_W^3 + m_Z^3}{4\pi v^3},\ T_0^2 = \frac{m_h^2 - \frac{3}{8\pi^2 v^2}(2m_W^4 + m_Z^4 - 4m_t^4)}{4D},$$
$$\lambda(T) = \lambda - \frac{3}{16\pi^2 v^4}\left(2m_W^4 \ln\frac{m_W^2}{A_B T^2} + m_Z^4 \ln\frac{m_Z^2}{A_B T^2} - 4m_t^4 \ln\frac{m_t^2}{A_F T^2}\right), \tag{2.44}$$

and where $A_B = 16\pi^2 \exp(-2\gamma_E) \approx 49.780$ and $A_F = \pi^2 \exp(-2\gamma_E) \approx 3.111$.

First of all, we see that the effective potential in equation 2.43 has received a temperature correction to the ω^2 term relative to the tree-level potential in equation 2.3. We also see that there is a cubic term, which is obviously not present at all at tree-level, and that the quartic coefficient has a weak temperature dependence. Let us for the moment neglect the term $ET\omega^3$ and the temperature dependence of λ. We immediately find that the stationary points of V_{tree} satisfy $\omega^2 = 0$ or $\omega^2 = -2D(T^2 - T_0^2)/\lambda$. For $T > T_0$, the only solutions is $\omega^2 = 0$, which is just the ground state at high temperature. On the other hand, for $T < T_0$, $\omega \equiv \omega_m = \sqrt{-2D(T^2 - T_0^2)/\lambda}$ is also a solution. We see that $V_{\text{eff}}(\omega_m, T) = -D^2(T^2 - T_0^2)/\lambda < V_{\text{eff}}(0, T)$. Thus, ω_m is the ground state of the system, and we say that a phase transition has occurred at the critical temperature $T_c = T_0$. If we let $\omega(T)$ denote the temperature dependent groundstate, we see that $\lim_{T\to T_c^-} \omega(T) = \lim_{T\to T_c^+} \omega(T) = 0$. Thus the phase transition is smooth, and is said to be a second order phase transition. See figures 1a and 1b, which show $V_{\text{eff}}(\omega, T)$ and $\omega(T)$, respectively, near the phase transition. We see that the potential has no barrier between ω and ω_m at $T = T_c$ and that $\omega(T)$ goes smoothly to zero at $T = T_c$.

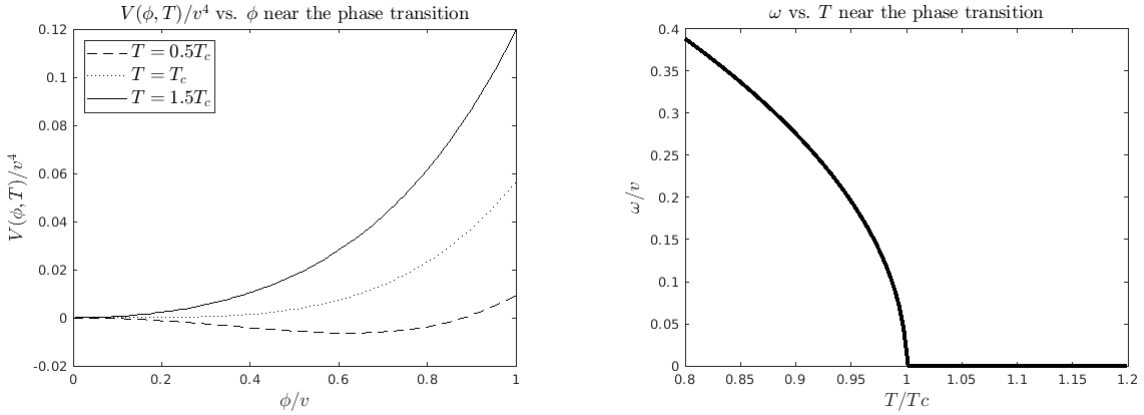

(a) Standard m_W, m_Z (b) Standard m_W, m_Z

Figure 1: Illustration of second order phase transition.

Let us now also consider the cubic term $ET\phi^3$ in the analysis (and less crucially the temperature dependence of λ) (again referring to [38]). By considering the stationary points of V_{eff}, we find that for low enough temperature, a local minimum appears at $\omega = \omega_m$ given by

$$\omega_m(T) = \frac{3ET}{2\lambda(T)} + \frac{1}{2\lambda(T)}\sqrt{9E^2T^2 - 8\lambda(T)D(T^2 - T_0^2)}. \tag{2.45}$$

We find that $V_{\text{eff}}(\omega_m, T = T_c) = 0$ at the critical temperature $T = T_c$, which is implicitly given by

$$T_c^2 = \frac{\lambda(T_c) D T_0^2}{\lambda(T_c) D - E^2}. \tag{2.46}$$

By solving equation 2.46 numerically, we can investigate the phase transition. In figures 2a and 2b we consider the phase transition for "standard" values of m_W and m_Z, i.e. the experimental values $m_W = 80.4$ GeV and $m_Z = 91.2$ GeV. We also use $m_h = 125.2$ GeV, $v = 246.22$ GeV and $m_t = 172.8$ GeV. Figure 2b clearly shows that $\omega(T)$ behaves very differently at $T = T_c$ compared to 1b. There is a discontinuity at $T = T_c$ of size $\Delta v_c / T_c \approx 0.17$, where $\Delta v_c / T_c$ denotes the order parameter

$$\frac{\Delta v_c}{T_c} = \frac{1}{T_c} \left(\lim_{T \to T_c^-} \omega(T) - \lim_{T \to T_c^+} \omega(T) \right) \tag{2.47}$$

We call such a phase transition a first order phase transition (FOPT).

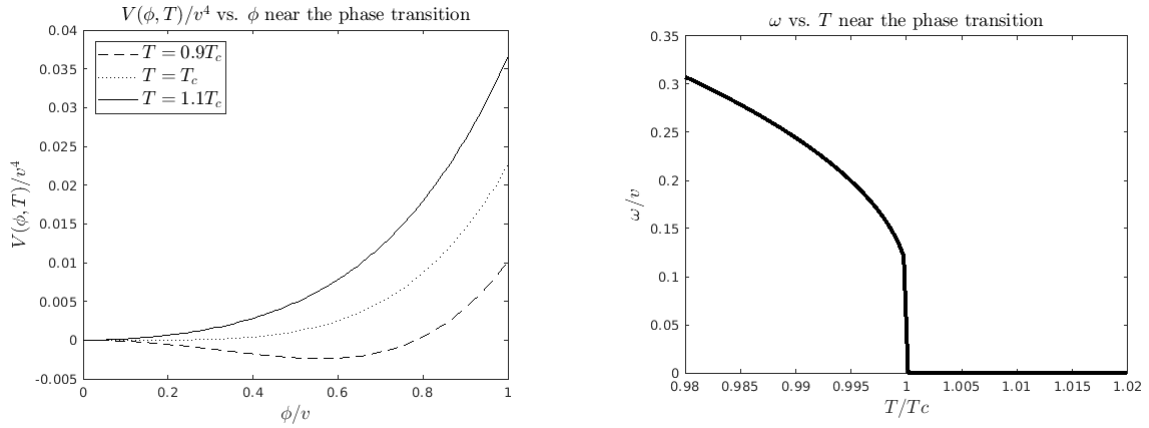

(a) V vs. ϕ (b) ω vs. T

Figure 2: Electroweak phase transition in the SM, as calculated from equation 2.43 with standard values of m_W, m_Z, i.e. $m_W = 80.4$ GeV and $m_Z = 91.2$ GeV.

In figures 3a and and 3b we again consider the phase transition, but use "modified" (i.e. non-experimental) values of m_W and m_Z, given by $m_W = m_Z = 250$ GeV. Referring to equation 2.44, we see that such a change increases the value of E relative to $\lambda(T)$, so we should expect to see a stronger transition, i.e. one which is more discontinuous. Indeed, this is what we see. Figure 3a clearly shows that at $T = T_c$ there is a potential barrier between the degenerate minima at $\phi = 0$ and $\phi = \omega_m$ (something which is difficult to see in 2a). The discontinuity in $\omega(T)$ is much more pronounced. The order parameter is found to be $\Delta v_c / T_c \approx 2.0$; a first order phase transition with $\Delta v_c / T_c \gtrsim 1$ is referred to as a strongly first order phase transition (SFOPT). For a strongly first order electroweak phase transition, we use the acronym SFOEWPT.

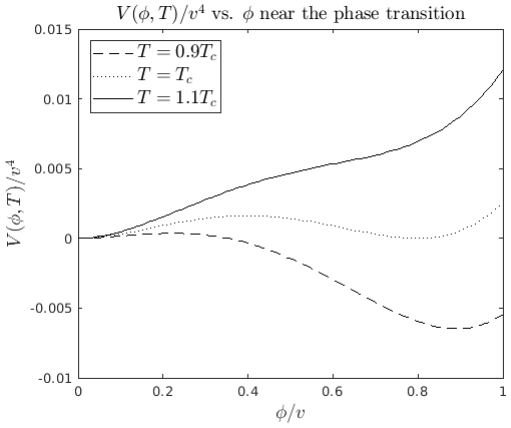

(a) V vs. ϕ

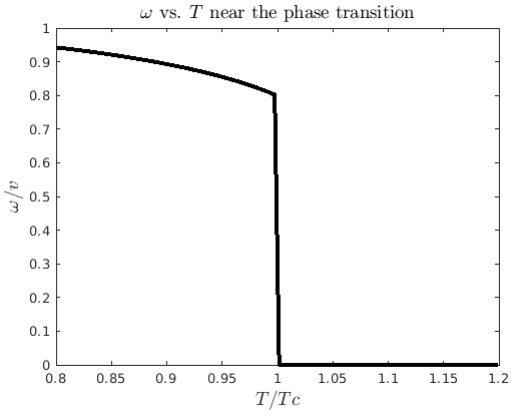

(b) ω vs. T

Figure 3: Electroweak phase transition in the SM, as calculated from equation 2.43 with modified values of m_W, m_Z, with $m_W = m_Z = 250$ GeV.

While somewhat simplified, the above analysis highlights the fact that a SFOEWPT is not possible in the SM [10, 11]. Thus, as mentioned already in the introduction, the SM cannot explain the baryon asymmetry, since the departure from thermal equilibrium is not strong enough (c.f. the Sakharov conditions in the introduction).

2.4.3 Phase transitions in 2HDMs

Let us now turn two phase transitions in 2HDMs. As already mentioned in the introduction, strong enough FOPTs can be realized in 2HDMs to satisfy the third Sakharov condition [16, 44], in contrast to the SM as illustrated in section 2.4.2. Phase transitions in 2HDMs have been studied in the literature, see e.g. [16, 36, 44]. We will not extensively review these works in this section, but rather present the setup for our calculations.

Thus, we consider a system with a tree-level potential given by equation 2.9, where the doublets Φ_1, Φ_2 are given in terms of the eight real scalar fields $\phi_1, ..., \phi_8$ by

$$\Phi_1 = \frac{1}{\sqrt{2}} \begin{pmatrix} \phi_1 + i\phi_2 \\ \phi_3 + i\phi_4 \end{pmatrix}, \quad \Phi_2 = \frac{1}{\sqrt{2}} \begin{pmatrix} \phi_5 + i\phi_6 \\ \phi_7 + i\phi_8 \end{pmatrix}. \tag{2.48}$$

We shall only consider $\mathcal{CP}$ and charge conserving vacua, which means that the background field $\boldsymbol{\omega}$ has the form $\boldsymbol{\omega} = (0, 0, \omega_3, 0, 0, 0, \omega_7, 0)$. At tree-level, $\boldsymbol{\omega} = \boldsymbol{v} \equiv (0, 0, v_1, 0, 0, 0, v_2, 0)$, where the vevs v_1 and v_2 have been defined in equation 2.10.

In analogy with the SM case, we can define an order parameter associated with the phase transitions. We can define such a parameter for a critical temperature (c) as well as for a nucleation temperature (n), the latter of which will be defined in equation 2.60. Thus, the order parameter $\Delta v_{c,n}/T_{c,n}$ is given by

$$\frac{\Delta v_{c,n}}{T_{c,n}} = \frac{1}{T_{c,n}} \left(\lim_{T \to T_{c,n}^-} \sqrt{\omega_3^2(T) + \omega_7^2(T)} - \lim_{T \to T_{c,n}^+} \sqrt{\omega_3^2(T) + \omega_7^2(T)} \right) \tag{2.49}$$

We treat the effective potential according to the Parwani method in equation 2.42. The bosonic modes that are summed over in $V_{\rm CW}^{\rm P}$ and $\Delta V_T^{\rm P}$ are the following: h, H, A, G^0, $H^\pm$ and $G^\pm$, as well as the longitudinal gauge boson modes W_L, Z_L and γ_L and the transverse gauge bosons modes W_T and Z_T. In the fermionic sector, we restrict ourselves to the third generation of quarks and leptons, since these are the heaviest and therefore have the largest influence on the effective potential. Thus we consider only t, b and τ and assume a Yukawa Lagrangian of the form

$$\begin{aligned}-\mathcal{L}_{\rm Yukawa} = &\begin{pmatrix}\bar{t}_L\\ \bar{b}_L\end{pmatrix}[a_b\Phi_1 + b_b\Phi_2]b_R + \begin{pmatrix}\bar{t}_L\\ \bar{b}_L\end{pmatrix}[a_t\tilde{\Phi}_1 + b_t\tilde{\Phi}_2]t_R\\ &+ \begin{pmatrix}\bar{\nu_\tau}_L\\ \bar{\tau}_L\end{pmatrix}[a_\tau\Phi_1 + b_\tau\Phi_2]\tau_R, + \text{ h.c.}\end{aligned} \tag{2.50}$$

where $\tilde{\Phi}_i = i\sigma_2\Phi_i^*$, $i = 1, 2$, denotes the charge conjugated field and where the coefficients a_f and b_f are related to the corresponding coefficients κ^f and ρ^f in equation 2.19 ($f = t, b, \tau$) according to

$$a_f = c_\beta\kappa^f - s_\beta\rho^f, \quad b_f = s_\beta\kappa^f + c_\beta\rho^f. \tag{2.51}$$

In the composite case, the Yukawa Lagrangian does not quite have the form in equation 2.50, due to the compositeness corrections, as described in equation 2.32. However, for simplicity we neglect this issue when calculating the phase transitions in C2HDM, as the phase transition does not depend very strongly on the fermion masses [6].

The degrees of freedom n_i which appear in $V_{\rm CW}^{\rm P}$ and $\Delta V_T^{\rm P}$ are given by

$$\begin{cases} n_h = 1,\ n_H = 1,\ n_A = 1,\ n_{G^0} = 1,\ n_{H^\pm} = 2,\ n_{G^\pm} = 2\\ n_{W_L} = 2,\ n_{Z_L} = 1, n_{\gamma_L} = 1, n_{W_T} = 4, n_{Z_T} = 2\\ n_t = 12,\ n_b = 12,\ n_\tau = 4.\end{cases}$$

For n_t, n_b and n_τ, there are four degrees of freedom due to the spin projections and due to counting both particles and anti-particles. For n_t and n_b, there is an additional factor of three due to the color degree of freedom. As for the renormalization constants, we recall that in the $\overline{\rm MS}$ scheme, $c_i = 1/2$ for the transverse modes and $c_i = 3/2$ for fermionic modes and longitudinal bosonic modes.

Finally, in order to calculate the effective potential we need the field and temperature dependent squared masses $m_i^2(\boldsymbol{\omega}, T)$. These have been calculated from the general expressions in [34], and are presented in appendix C. As for the counterterms, the most general counterterm potential in 2HDM has the same form as in equation 2.9, with the parameters $m_{ij}^2 \to \delta m_{ij}^2$ and $\lambda_i \to \delta\lambda_i$. As discussed in section 2.4.1, issues arise when imposing the second counterterm condition in equation 2.35 due to the Goldstone modes. Another, more practical issue, is that in order to correctly implement the counterterm conditions in equation 2.35 in all directions in field space, we would need to know the field dependent masses

[6] Recall that the fermionic integral J_-, unlike the bosonic one J_+, does not have a cubic term (see equation 2.39).

$m_i^2(\boldsymbol{\phi}, T)$ not just for $\boldsymbol{\phi} = \boldsymbol{\omega}$ but also for $\boldsymbol{\phi} \neq \boldsymbol{\omega}$. In the latter case, the diagonalization cannot be done by hand. Because of these issues, we will use a simplified counterterm potential of the form

$$V_{\mathrm{CT}}(\boldsymbol{\omega}) = \frac{1}{2}\delta m_{11}^2 \omega_3^2 + \frac{1}{2}\delta m_{22}^2 \omega_7^2. \tag{2.52}$$

We only impose the first of the counterterm conditions in equation 2.35 on this potential, and we will only impose the condition in those directions in field space that get a vev, i.e. ϕ_3 and ϕ_7. This yields the following equations form the parameters δm_{11}^2 and δm_{22}^2, which can be evaluated using $m_i^2(\boldsymbol{\omega}, T)$ rather than the general $m_i^2(\boldsymbol{\phi}, T)$

$$\begin{cases} \delta m_{11}^2 = -\dfrac{1}{v_1}\dfrac{\partial V_{\mathrm{CW}}}{\partial \omega_3}\Big|_{\boldsymbol{\omega}=\boldsymbol{v}} & \text{if } v_1 \neq 0, \quad \delta m_{11}^2 = 0 \text{ if } v_1 = 0, \\ \delta m_{22}^2 = -\dfrac{1}{v_2}\dfrac{\partial V_{\mathrm{CW}}}{\partial \omega_7}\Big|_{\boldsymbol{\omega}=\boldsymbol{v}} & \text{if } v_2 \neq 0, \quad \delta m_{22}^2 = 0 \text{ if } v_2 = 0. \end{cases} \tag{2.53}$$

2.4.4 Dynamics of cosmological first order phase transition

Thus far, we have characterized phase transitions in terms of the critical temperature. However, we have said nothing about the dynamics of the transition from the old (initial, false) to the new (final, true) vacuum. In this section, we briefy describe the dynamics of a first order cosmological phase transition.

As we have seen, for a first order phase transition there is a potential barrier separating the false vacuum and the true vacuum. As the temperature drops below the critical temperature, the false vacuum becomes metastable. The transition from the false vacuum to the true vacuum takes place through thermal jumps and quantum tunneling across the barrier [45, 46, 47]. Because these processes are of a random nature, the transition does not happen homogeneously throughout space, but appears as the nucleation of "bubbles" of the true vacuum; this is schematically illustrated in figure 4 below.

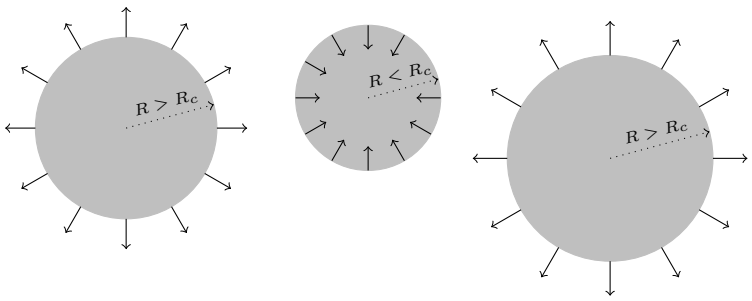

Figure 4: Illustration of the bubble nucleation in a first order cosmological phase transition. Lightgray represents the true vacuum and the white background represents the false vacuum. R denotes the bubble radius and R_c denotes the critical bubble radius.

Let us first gain a qualitative understanding of the bubble dynamics by considering the so-called thin-wall approximation [46]. This approximation applies when the energy difference

$\Delta V_{\text{eff}} = V_{\text{eff}}(\boldsymbol{\omega}_i) - V_{\text{eff}}(\boldsymbol{\omega}_f) > 0$ between the initial and the final vacuum, $\boldsymbol{\omega}_i$ and $\boldsymbol{\omega}_f$ respectively, is small. In the thin-wall approximation, the scalar field $\boldsymbol{\phi}$ changes on a small lengthscale, say d, from the initial vacuum inside the bubble to the final vacuum far away from the bubble. Under these conditions, the "bubble" really is a bubble, with a well-defined radius R (in the limit $\Delta V_{\text{eff}} \to 0$) and a wall of thickness $d << R$. In this approximation, the free energy of the bubble can be attributed to two terms: a volume term and a surface term. The volume term simply corresponds to the free energy of the inside (true vaccum) of the bubble relative to the outside (false vacuum), and is given by $-(4\pi/3)R^3\Delta V_{\text{eff}}$. Meanwhile, the surface term is due the change in free energy between the inside and outside of the bubble over the lengthscale d at the surface of the bubble. Because $d << R$, the description of this term as a surface term is sensible, and it can be written in the form $4\pi R^2\mu$, where μ denotes the surface tension (which can be calculated from V_{eff} in the thin-wall approximation $\Delta V_{\text{eff}} \to 0$). Hence the free energy F of the bubble, in the thin-wall approximation, has the form (see also [47, 40])

$$F = -\frac{4\pi}{3}R^3\Delta V_{\text{eff}} + 4\pi R^2\mu. \tag{2.54}$$

If R is large enough the volume term dominates and the bubble will grow, while if R is below a certain critical [7] value R_c the surface term dominates and the bubble collapses. From equation 2.54, solving $\partial F/\partial R = 0$ for R, we immediately obtain

$$R_c = \frac{2\mu}{\Delta V_{\text{eff}}}. \tag{2.55}$$

In general, i.e. not necessarily in the thin-wall approximation, the critical bubble is determined [45, 46] by extremizing the Euclidean action [8] S_E, given by [9],

$$S_E = \begin{cases} S_4 = 2\pi^2 \displaystyle\int r^3 dr \left[\frac{1}{2}\left(\frac{d\boldsymbol{\phi}}{dr}\right)^2 + V_{\text{eff}}(\boldsymbol{\phi}, 0)\right], \ T = 0, \\ S_3 = 4\pi \displaystyle\int r^2 dr \left[\frac{1}{2}\left(\frac{d\boldsymbol{\phi}}{dr}\right)^2 + V_{\text{eff}}(\boldsymbol{\phi}, T)\right], \ T > 0. \end{cases} \tag{2.56}$$

In S_3, the r coordinate is simply given by $r = |\boldsymbol{x}|$, where $\boldsymbol{x}$ denotes the vector of spatial coordinates, whereas in S_4, the r coordinate is given by $r = \sqrt{t^2 + |\boldsymbol{x}|^2}$. In practice, our calculations will be done in the finite temperature regime, so that S_3 is the appropriate Euclidean action.

The corresponding equations of motion from the Euclidean action are [46]

$$\begin{cases} \dfrac{d^2\boldsymbol{\phi}}{dr^2} + \dfrac{3}{r}\dfrac{d\boldsymbol{\phi}}{dr} = \nabla V_{\text{eff}}(\boldsymbol{\phi}, 0), \ \ T = 0, \\ \dfrac{d^2\boldsymbol{\phi}}{dr^2} + \dfrac{2}{r}\dfrac{d\boldsymbol{\phi}}{dr} = \nabla V_{\text{eff}}(\boldsymbol{\phi}, T), \ T > 0, \end{cases} \tag{2.57}$$

[7] This is unrelated to critical in the sense of the critical temperature.

[8] We simply use S_E as a symbol to denote either S_4 or S_3, according to whether $T = 0$ or $T \neq 0$.

[9] We assume spherical symmetry for the bubble.

subject to the boundary conditions $\boldsymbol{\phi} \to 0$ as $r \to \infty$ and $d\boldsymbol{\phi}/dr|_{r=0} = 0$. Solving the appropriate equation of motion in the respective temperature regime and substituting into equation 2.56, the Euclidean action of the extremal solution is obtained.

For the Euclidean action of the extremal solution, the critical bubble action S_c is then given by

$$S_c = \begin{cases} S_4, & T = 0, \\ S_3/T, & T > 0. \end{cases} \tag{2.58}$$

With these definitions in place, the nucleation rate per unit volume Γ/V of bubbles above the critical size is given by [46, 47, 48]

$$\Gamma/V = Ae^{-S_c}. \tag{2.59}$$

The coefficient A can be calculated [49, 46], but it is quite difficult to do so. On dimensional grounds, $A \sim T^4$ and for the electroweak phase transition, $A \approx e^{-14}T^4$ [50, 47].

We have previously defined the critical temperature. However, this does not necessarily adequately describe the temperature at which the cosmological phase transition takes place due to i) the dynamics of the bubble nucleation and ii) the expansion of the universe. Instead, the onset of the cosmological phase transition occurs at the nucleation temperature T_n [48, 50], which is defined by the condition that there is approximately one bubble nucleated per horizon volume. This translates to the approximate condition [48, 50]

$$S_c(T = T_n) \approx 140, \tag{2.60}$$

which implicitly determines the nucleation temperature. Henceforth we will use the nucleation temperature to characterize the temperature at which the cosmological phase transition takes place. This should be adequate unless the transition exhibits strong supercooling, in which case the so-called percolation temperature is more adequate; see [48, 50].

Aside from the nucleation temperature, the key parameters that characterize the phase transition are the strength parameter α and the inverse duration of the phase transition per Hubble time, β/H [10]. More precisely, α is given by (following the convention in [48, 50]) the ratio of the volume density of the energy released through the phase transition and the radiation energy density ρ_{rad} of the plasma, and can be calculated from the effective potential according to [51]

$$\alpha = \frac{1}{\rho_{\text{rad}}} \left[V_i - V_f - \frac{T}{4} \left(\frac{\partial V_i}{\partial T} - \frac{\partial V_f}{\partial T} \right) \right] \Bigg|_{T=T_n}. \tag{2.61}$$

Here, $V_{i,f}$ is shorthand for $T \mapsto V_{\text{eff}}(\boldsymbol{\omega}_{i,f}, T)$, i.e. the effective potential as a function of temperature evaluated for the initial (false) and final (true) vacuum respectively. The radiation energy density ρ_{rad} is given by

$$\rho_{\text{rad}}(T = T_n) = g_* \frac{\pi^2}{30} T_n^4, \tag{2.62}$$

[10] Thus β denotes the inverse duration, but we will always express this in terms of the Hubble time and only work with the ratio β/H.

where g_* is the effective number of relativistic degrees of freedom around nucleation. With a SM particle content, $g_* \approx 106.75$ at the relevant temperatures above the electroweak temperature ~ 100 GeV; we will use the value $g_* \approx 106.75$ throughout. For a discussion about the effective number of relativistic degrees of freedom, see [52]. Meanwhile, the parameter β/H can be calculated from the critical bubble action $S_c = S_3/T$ according to [48]

$$\beta/H = T_n \left. \frac{\partial(S_3/T)}{\partial T} \right|_{T=T_n}. \tag{2.63}$$

From α and β/H we can define two additional parameters, which will be useful later on, namely the ratio K of kinetic energy in the plasma and the initial bubble energy, and the mean bubble separation D at nucleation [11]. First let us also introduce the parameter v_w, which denotes the bubble wall velocity. In principle this can be calculated (see e.g. [53]), but such calculations are rather involved. In our numerical simulations, to be later discussed, we will instead treat v_w as a "free" parameter and consider how it affects the amplitude of the gravitational wave spectrum in two extreme cases. In terms of α and v_w, the kinetic energy fraction K is then given by [50] [54]

$$K = \frac{\kappa\alpha}{1+\alpha}, \tag{2.64}$$

where κ is an efficiency factor [54] which depends on α and v_w, and which is minimized at $v_w = 1$ and maximized at $v_w = v_{\mathrm{CJ}}$, where v_{CJ} denotes the so-called Chapman-Jouguet speed. Finally, assuming that the bubbles expand as detonations [12], i.e. if $v_w > c_s$, with $c_s = 1/\sqrt{3}$ denoting the speed of sound of the plasma, the mean bubble separation D at nucleation satisfies [50]

$$HD = \frac{(8\pi)^{1/3}}{\beta/H}. \tag{2.65}$$

Note that the velocities (v_w, v_{CJ} and c_s) are given in natural units, i.e. normalized to the speed of light. The value $c_s = 1/\sqrt{3}$ for the speed of sound in the plasma, follows from the radiation equation of state, $p(\rho) = \rho/3$, and the definition $c_s = \sqrt{\partial p/\partial\rho}$. See e.g. [54] for further details on the hydrodynamics of the phase transition.

2.5 Gravitational waves from cosmological phase transitions

As we have discussed in the previous section, a cosmological first order phase transition proceeds through the nucleation of expanding bubbles of the true vacuum. The collisions between such bubbles induce shear stresses in the cosmological plasma, leading to the production of gravitational waves [48]. Because the bubble collisions sourcing the gravitational waves occur randomly throughout the universe at the time of the phase transition, the gravitational waves due to a cosmological phase transition would appear as a stochastic

[11] Typically this is denoted by R, but we have used this letter for the bubble radius.

[12] We will only consider the case of detonations.

gravitational wave background, akin to the cosmic microwave background of photons from the time of photon decoupling in the early universe. We will quantify this gravitational wave background by the power spectrum of the gravitational wave density, denoted by $h^2\Omega_{\mathrm{GW}}(f)$ and defined by

$$h^2\Omega_{\mathrm{GW}}(f) = h^2\frac{d(\rho_{\mathrm{GW}}/\rho_c)}{d\ln f}, \tag{2.66}$$

where f denotes the frequency, ρ_{GW} the gravitational wave energy density, ρ_c the critical density today and where h is defined through $H_0 = 100h$ kms^{-1}Mpc^{-1}, with H_0 denoting the Hubble constant today [13]. This is the notation used in e.g. [48, 50].

There are three main processes associated with the bubble dynamics that source the gravitational waves [48], namely:

- Collisions of bubble walls.
- Sound waves in the plasma.
- Turbulence due to magnetohydrodynamic effects.

Consequently, the power spectrum can be decomposed as

$$h^2\Omega_{\mathrm{GW}} = h^2\Omega_{\mathrm{GW,coll}} + h^2\Omega_{\mathrm{GW,sw}} + h^2\Omega_{\mathrm{GW,turb}}, \tag{2.67}$$

with $h^2\Omega_{\mathrm{GW,coll}}$, $h^2\Omega_{\mathrm{GW,sw}}$ and $h^2\Omega_{\mathrm{GW,turb}}$ representing the collision, sound wave and turbulence processes, respectively.

As argued in [50], unless the bubble wall velocity undergoes runaway acceleration, corresponding to $v_w \to 1$, the collision contribution to the gravitational wave density will not be very significant compared to the soundwave and turbulence contributions. In the subsequent analysis, we therefore disregard the collision term. We will also disregard the turbulunce term, due to the theoretical uncertainties in its contribution. As argued in [50] the turbulence contribution cannot be larger than the sound wave contribution. Thus we get a conservative, but not unreasonably so, estimate of the gravitational wave signal.

The state-of-the-art expressions for the soundwave contribution $h^2\Omega_{\mathrm{GW,sw}}$, subsequently simply denoted by $h^2\Omega_{\mathrm{GW}}$, is given in [50]. The power spectrum has the form

$$h^2\Omega_{\mathrm{GW}}(f) = (h^2\Omega_{\mathrm{GW}})_{\mathrm{peak}}C(f/f_{\mathrm{peak}}), \tag{2.68}$$

where C denotes the spectral shape function, given by

$$C(s) = s^3\left(\frac{7}{4+3s^2}\right)^{7/4}, \tag{2.69}$$

f_{peak} denotes the peak frequence given by

$$f_{\mathrm{peak}} = 26\left(\frac{1}{HD}\right)\left(\frac{T_n}{100\text{ GeV}}\right)\left(\frac{g_*}{100}\right)^{1/6}\ \mu\mathrm{Hz}, \tag{2.70}$$

[13] We will use the value $h = 0.678$ from the 2015 Planck data [55]

and where $(h^2\Omega_{\mathrm{GW}})_{\mathrm{peak}}$ denotes the peak amplitude, given by

$$(h^2\Omega_{\mathrm{GW}})_{\mathrm{peak}} = \begin{cases} 2.453 \cdot 10^{-7} \cdot \left(\frac{100}{g_*}\right)^{1/3} \left(\frac{HD}{\sqrt{c_s}}\right)^2 K^{3/2}, \ H\tau_{\mathrm{sh}} < 1 \\ 2.453 \cdot 10^{-7} \cdot \left(\frac{100}{g_*}\right)^{1/3} \left(\frac{HD}{c_s}\right) K^2, \ H\tau_{\mathrm{sh}} > 1, \end{cases} \tag{2.71}$$

where $H\tau_{\mathrm{sh}} = HD/\sqrt{K}$ denotes the shock formation timescale. In equations 2.70 and 2.71, the parameters α and β/H, defined in equations 2.61 and 2.63 respectively, enter through equations 2.64 and 2.65.

From equation 2.68 we can compute the power spectrum of a given model realization; an example of such a power spectrum is given in figure 6 in the results section 4.1. An important quantity to quantify whether the associated gravitational wave signal will be observable by a given detector is the signal-to-noise-ratio (SNR), given by [48, 50]

$$\mathrm{SNR} = \sqrt{\mathcal{T} \int_{f_{\mathrm{min}}}^{f_{\mathrm{min}}} df \left[\frac{h^2\Omega_{\mathrm{GW}}(f)}{h^2\Omega_{\mathrm{Sens}}(f)}\right]^2}. \tag{2.72}$$

Here, $h^2\Omega_{\mathrm{Sens}}$ is the power spectrum of the sensitivity function for a given detector, f_{min} and f_{max} denote the endpoints of the frequency range of the detector, and $\mathcal{T}$ denotes the duration of data collection. For the sensitivity curves, we refer to [56]. In the same reference, the notions of peak-integrated sensitivity (PIS) and peak-integrated sensitivity curve (PISC) are introduced. The PIS $h^2\Omega_{\mathrm{PIS}}(f_{\mathrm{peak}}; \mathcal{T})$ approximately determines, as a function of peak frequency f_{peak} and for a given duration $\mathcal{T}$, the SNR according to

$$\mathrm{SNR}_{\mathrm{PIS}} = \frac{(h^2\Omega_{\mathrm{GW}})_{\mathrm{peak}}}{h^2\Omega_{\mathrm{PIS}}(f_{\mathrm{peak}}; \mathcal{T})}. \tag{2.73}$$

The associated PISC is then simply the graph of the map $f_{\mathrm{peak}} \mapsto h^2\Omega_{\mathrm{PIS}}(f_{\mathrm{peak}}; \mathcal{T})$. We will consider the PISCs of the LISA [21], BBO [22] and DECIGO [23] detectors.

3 Implementation

3.1 `2HDMC`

Our implementation of 2HDMs is based on `2HDMC` [26] (two-Higgs-doublet model calculator), which is a `C++` program that implements the $\mathcal{CP}$-conserving E2HDM, using the basis invariant formalism presented in [27, 28].

The program features different model parametrizations, notably the general basis, Higgs basis, physical basis and hybrid basis. The former two were presented in section 2.2. The physical basis [26] is defined by the parameters m_h, m_H, m_A, $m_H^{\pm}$, $s_{\beta-\alpha}$, λ_6, λ_7, m_{12}^2 and t_β; thus, conversion to the physical basis calculates the masses of the Higgs bosons. Finally,

the hybrid basis [57] is defined by the parameters m_h, m_H, $c_{\beta-\alpha}$, t_β as well as the quartic couplings Z_4, Z_5 and Z_7 in the Higgs basis [14]. The convenience of this basis lies in the fact that we can easily incorporate phenomenological constraints, by putting m_h close to the mass ≈ 125 GeV of the observed Higgs boson, and $s_{\beta-\alpha}$ close to 1, corresponding to the alignment limit discussed in section 2.2.

Further, `2HDMC` provides functionality to check stability, unitarity and perturbativity of the potential (see section 3.3 below), calculates decay widths of Higgs bosons, and calculates the oblique parameters S, T, U, V, W and X [58] (see section 3.3 below).

In order to implement the C2HDM, a slightly modified version of `2HDMC`, `C2HDMC`, was made. `C2HDMC` implements the compositeness modifications to the gauge and Higgs boson couplings in table 4, the Higgs self couplings (see [19] and the example in equation 2.28) as well as the Yukawa couplings in equation 2.29.

3.2 `CosmoTransitions`

`CosmoTransitions` [42] is a `Python` package for analyzing the phase structure of scalar potentials. To implement a model, the tree-level potential V_{tree} along with a potential counterterm V_{CT} potential have to specified. In addition, the temperature and field dependent masses $m_i^2(\boldsymbol{\omega}, T)$ for bosons and fermions must be provided. The effective potential V_{eff} is calculated according to the Parwani method in equation 2.42.

At each temperature T, the program approximately solves the equations of motion in equation 2.57, and thereby determines the Euclidean action in equation 2.56. From equations 2.58 and 2.60 the nucleation temperature is determined for each transition that is found for the given potential. There is also an option to calculate the critical temperature for the transitions.

3.3 Constraints

3.3.1 Theoretical constraints

For a realization of 2HDM to be realistic, a reasonable requirement is that the vacuum be stable. We call this constraint positivity/stability (of the potential). In the case of an elementary 2HDM, this constraint requires that the potential be positive for arbitrary large field values in all directions in field space. The conditions of this requirement have been calculated in [59] and are implemented in `2HDMC`. In the composite case, we also wish to require stability of the vacuum. However, in the composite case we do *not* impose the constraint that the calculated potential be positive at arbitrarily large field values. The reason is that the potential has been calculated as an expansion in v/f, and when either of the vevs v_1, v_2 tend to infinity, this expansion breaks down. Hence, in the composite case, it would not make sense to impose the stability constraints on the parameters if the potential that would be imposed in the elementary case. Indeed, as we will see in section

[14] For the hybrid basis, we use the notation $Z_{4,5,7}$ rather than $\Lambda_{4,5,7}$ for the quartic couplings in the Higgs basis.

4.2, in the composite case we often have $\lambda_1 < 0$ or $\lambda_2 < 0$; such values violate the stability conditions imposed in the elementary case.

Another important theoretical constraint is the unitary of the scattering matrix, $\mathcal{S}$. A conservative requirement, appropriate in a weakly coupled theory, is that the scattering matrix be unitary at tree-level. The corresponding conditions have been calculated in [60], and are implemented in `2HDMC`. Below, we will simply refer to this constraint as unitarity.

Finally, in order not to violate perturbativity, the condition $|\lambda_{h_i h_j h_k h_l}| \leq 4\pi$ is imposed on all quartic Higgs self couplings, as defined in equation 2.18 [26]. This constraint is also implemented in `2HDMC`.

3.3.2 Experimental constraints

`HiggsBounds` [61, 62, 63, 64, 65, 66] is a tool for testing the Higgs sectors of BSM models. It compares Higgs masses, Higgs boson decay widths, branching ratios and production cross sections calculated in such models to experimental data from LEP, the Tevatron and LHC, in order to determine if a model realization is excluded at 95% confidence level (CL) or not. Thus, we implement experimental constraints on the Higgs sector by demanding that a given point in parameter space be allowed by `HiggsBounds`.

The related tool `HiggsSignals` [67, 68, 69] also confronts BSM Higgs sectors with experimental data. It calculates a χ^2 measure of how well the calculated Higgs masses and signal rates fit with experimental data from the Tevatron and LHC. A p-value for testing the null hypothesis that the calculated values agree with the experimental ones is also calculated. Thus, we implement the experimental constraint from `HiggsSignals` by saying that a point is *not* admissible if the calculated p-value is below some cutoff, which we will take to be 0.05. In `HiggsSignals` one can specify so-called theoretical mass uncertainties for the Higgs bosons. These parameters reflect uncertainties of the calculated Higgs boson masses from a certain model. In the simulations, we set these uncertainties to 5 GeV for all the Higgs bosons; the value of 5 GeV is chosen to be consistent with the mass window that we allow for m_h in C2HDM, as discussed in section 3.5.

In the following, we will often use the abbreviation `HB/HS` to refer to the constraints from `HiggsBounds` and `HiggsSignals`, respectively.

3.3.3 Oblique parameters

In addition to the constraints from `HiggsBounds` and `HiggsSignals`, we constrain the model experimentally through the so-called oblique parameters. The original oblique parameters are denoted S, T and U and are also referred to as the Peskin-Takeuchi parameters [30]. In [58], the additional oblique parameters V, W and X are defined. The oblique parameters can be measured by probing the electroweak sector, and are defined in such a way that they are equal to zero for the SM. In this sense, they quantify BSM physics in the electroweak sector. On the other hand, for a particular model the oblique parameters can be calculated; the calculation of the full set of oblique parameters is implemented in

2HDMC. Thus, experimental data on the oblique parameters can be used as a constraint on model realizations.

We have implemented the constraint from the oblique parameters by using the 90% CL (approximate) ellipse in the ST-plane (setting $U = 0$), that is shown in figure 10.6 in [70]. This is the same approach as used in [71]. The equation for the approximate ellipse $\mathcal{E}_{ST}$ has been extracted by measurements in the figure. Data points along the contour, kindly provided by [72], are confirmed to fit well to this equation, given by

$$\mathcal{E}_{ST} = \left\{ S, T \in \mathbb{R} \,\middle|\, 1 = \left(\frac{\tilde{S}c_\theta + \tilde{T}s_\theta}{a} \right)^2 + \left(\frac{-\tilde{S}s_\theta + \tilde{T}c_\theta}{b} \right)^2 \right\}, \tag{3.1}$$

where $\tilde{S} = S - S_0$, $\tilde{T} = T - T_0$, $S_0 = 0.00$, $T_0 = 0.005$, $\theta = 0.595$, $a = 0.1458$ and $b = 0.0437$. The constraint due to the ST-ellipse $\mathcal{E}_{ST}$ is then that a model realization is admissible if the point (S, T) lies inside of $\mathcal{E}_{ST}$, where S and T denote the values of the S and T parameters calculated for the model realization in question.

3.4 Implementation of E2HDM

A Python program, E2HDM_CT.py, was written to implement the E2HDM for the purpose of studying its phase transitions. E2HDM_CT.py subclasses the function genericpotential.py in CosmoTransitions, and specifies the tree-level potential V_{2HDM} and the field and temperature dependent masses $m_i^2(\boldsymbol{\omega}, T)$, as discussed in section 2.4.3 and appendix C. Using the functionality supplied by CosmoTransitions, E2HDM_CT.py calculates the transitions of a particular realization of 2HDM, and records the nucleation temperature T_n, critical temperature T_c as well as the phase discontinuities Δv_n and Δv_c for each transition. In addition, the α and β/H parameters are calculated according to equations 2.61 and 2.63.

Further, a C++ program, ElRunCT, was written to implement a E2HDM in the hybrid basis. The program generates model realizations by randomly picking parameter values according to

$$\begin{aligned} &m_h/\text{GeV} \in (120, 130),\ m_H/\text{GeV} \in (150, 800),\ \sin(\beta - \alpha) \in (0.95, 0.999), \\ &\ln\tan(\beta) \in (-\ln(10), \ln(10)),\ Z_{4,5,7} \in (-3, 3), \rho_t \in (-1 \cdot \kappa_t, 1 \cdot \kappa_t), \\ &\rho_b \in (-10 \cdot \kappa_b, 10 \cdot \kappa_b),\ \rho_\tau \in (-10 \cdot \kappa_\tau, 10 \cdot \kappa_\tau). \end{aligned} \tag{3.2}$$

These parameter ranges are selected to provide points which are likely to pass experimental constraints. For the constraints in the Yukawa sector, we refer to [73].

A 2HDMC object is constructed with the given parameters in the hybrid basis, and perturbativity, unitarity and positivity/stability constraints are imposed on the model, as described in section 3.3. The masses of the Higgs bosons and the oblique parameters are calculated through 2HDMC. For an admissible model, the HiggsBounds and Higgssignals experimental constraints are imposed, with a limit of 0.05 used for the p-value for all simulations. We also take the experimental constraint from the $\mathcal{E}_{ST}$ ellipsis into account. However, we do not impose it during the simulations, but only afterwards during plotting.

If a model passes both the theoretical and experimental constraints, the model is passed to `E2HDM_CT.py` to find the phase transitions and calculate the phase transition parameters. The SNR value for the LISA detector is then calculated numerically according to equation 2.72 by numerical integration. Finally, the data is written to a simple textfile.

3.5 Implementation of C2HDM

Another `Python` program, `C2HDM_CT.py`, was written to implement the C2HDM for the purpose of studying its phase transitions. The program `C2HDM_CT.py` is identical to the program `E2HDM_CT.py`, described above, aside from imposing the criterion that a phase is discarded if the magnitude of $\boldsymbol{\omega}$ at any point exceeds the composite energy scale parameter f. This is to ensure that we do not analyze phases beyond the region where the expansion in v/f, in which the C2HDM is formulated, remains valid.

Further, a `C++` program, `CompRunCT`, was written to implement the C2HDM. The program randomly generates model realizations by the picking the (scaled) compositeness parameters uniformly according to

$$\begin{aligned} &f/\text{GeV} \in (600, 3000),\ g_\rho \in (2, 10),\ X \in (0, 10),\ \text{where} \\ &X = Y_1^{12}/f,\ Y_2^{12}/f,\ \Delta_L^1/f,\ \Delta_R^2/f,\ M_\Psi^{11}/f,\ M_\Psi^{22}/f,\ M_\Psi^{12}/f. \end{aligned} \tag{3.3}$$

These are the same ranges as those used in [19]. Then, the potential parameters m_{11}^2, m_{22}^2, m_{12}^2 and $\lambda_1, ..., \lambda_7$ are calculated according to equation 2.22. See appendix B.2 for details on this calculation, which was implemented in a utility program `CompUtil`. Given the potential parameters, the basis angle β and the vev v are implicitly determined by the tadpole equations in 2.11. Eliminating v from the tadpole equations, we obtain a quartic equation for t_β,

$$a_4 t_\beta^4 + a_3 t_\beta^3 + a_2 t_\beta^2 + a_1 t_\beta + a_0 = 0, \tag{3.4}$$

where the parameters a_i, $i = 0, ..., 4$ are given by

$$\begin{cases} a_0 = -\lambda_1 m_{12}^2/f^2 - \lambda_6 m_{11}^2/f^2 \\ a_1 = -\lambda_{345} m_{11}^2/f^2 + \lambda_1 m_{22}^2/f^2 - 2\lambda_6 m_{12}^2/f^2 \\ a_3 = -3\lambda_7 m_{12}^2/f^2 + 3\lambda_6 m_{22}^2/f^2 \\ a_3 = -\lambda_2 m_{12}^2/f^2 + \lambda_{345} m_{22}^2/f^2 + 2\lambda_7 m_{12}^2/f^2 \\ a_4 = \lambda_7 m_{22}^2/f^2 + \lambda_2 m_{12}^2/f^2 \end{cases}. \tag{3.5}$$

The solution of the quartic equation 3.4 was implemented using Ferrari's method [74]. Given t_β, the vev v is then determined from the tadpole equations in 2.11, both of which determine v^2. Taking the average of the two conditions, v is calculated according to

$$v^2 = \frac{m_{12}^2 t_\beta - m_{11}^2}{\lambda_1 c_\beta^2 + \lambda_{345} s_\beta^2 + 3\lambda_6 s_\beta c_\beta + \lambda_7 s_\beta^2 t_\beta} + \frac{m_{12}^2 t_\beta^{-1} - m_{22}^2}{\lambda_2 s_\beta^2 + \lambda_{345} c_\beta^2 + \lambda_6 c_\beta^2 t_\beta^{-1} + 3\lambda_7 s_\beta c_\beta}. \tag{3.6}$$

We check that both tadpole conditions are satisfied for this value of v within a narrow tolerance.

Having calculated v, the SM vev v_{SM} is in principle determined by equation 2.23. However, it may happen that the value $v_{\text{SM}}^{\text{calc}}$ which is calculated from equation 2.23 in this way differs from the experimental value $v_{\text{SM}} = 246.22$ GeV. In the simulations, we allow these values to differ by at most 2% of v_{SM}. We also require that the vev v satisfy $|v| < f$, in order for the expansion in v/f to be valid.

The C2HDM realization obtained through the calculations described above is then constructed as a `C2HDMC` object in the general basis, and the masses of the Higgs bosons are calculated through `C2HDMC`. When doing so, we make sure that all squared masses are positive, to ensure that values of t_β and v found above actually correspond to a (local) minimum of the potential. Unlike the elementary case, we do *not* impose the positivity/stability constraint on the potential, as explained in section 3.3. Further, we check that the mass m_h satisfies $m_h/\text{GeV} \in (120, 130)$, i.e. approximately within 5 GeV of the value 125 GeV for the mass of the observed Higgs boson. In a similar spirit, we check that the top mass m_t, as calculated from equation B.4, satisfies $m_t/\text{GeV} \in (165, 175)$.

As in the elementary case, we also impose the constraints due to `HiggsBounds` and `HiggsSignals`, as well as the constraints on the oblique parameters from the $\mathcal{E}_{ST}$ ellipse. If the model is admissible, it is passed to `C2HDM_CT.py` in order to find the phase transitions and calculate the phase transition parameters. The SNR value is calculated in the same way as in the elementary case.

4 Results

4.1 E2HDM

First of all, we illustrate the impact of the experimental constraints described in section 3.3.2. Figure 5 below shows scatter plots in the ST-plane along with the ST-ellipse $\mathcal{E}_{ST}$ and the SNR value in colour code for two cases: without `HB/HS` constraints (5a) and with `HB/HS` constraints (5b). Let us first remark on the convention we use when plotting the SNR value. Unless stated otherwise, it is computed conservatively for the LISA detector by setting $v_w = 1$ and with a duration $\mathcal{T} = 9.5 \cdot 10^7$ s (corresponding to 4 years with a 75% duty cycle, as done in [50]). Points with SNR < 1 are shown in grey, while points with SNR ≥ 1 are color coded according to the SNR value. We see that applying the `HB/HS` constraints removes several points with high SNR (as well as several points with low SNR). Further adding the constraint from the ST-ellipse removes most points overall, but does leave four points with high SNR [15] Henceforth, unless stated otherwise, the experimental constraints both from `HB/HS` and the ST-ellipse will be applied. The theoretical constraints from positivity/stability, unitarity and perturbativity are always applied.

[15] In total, there were around $6.1 \cdot 10^4$ points. Of these, around $4.0 \cdot 10^4$ points passed the `HB/HS` constraints, and around $1.3 \cdot 10^4$ points passed the constraints from `HB/HS` and the ST-ellipse.

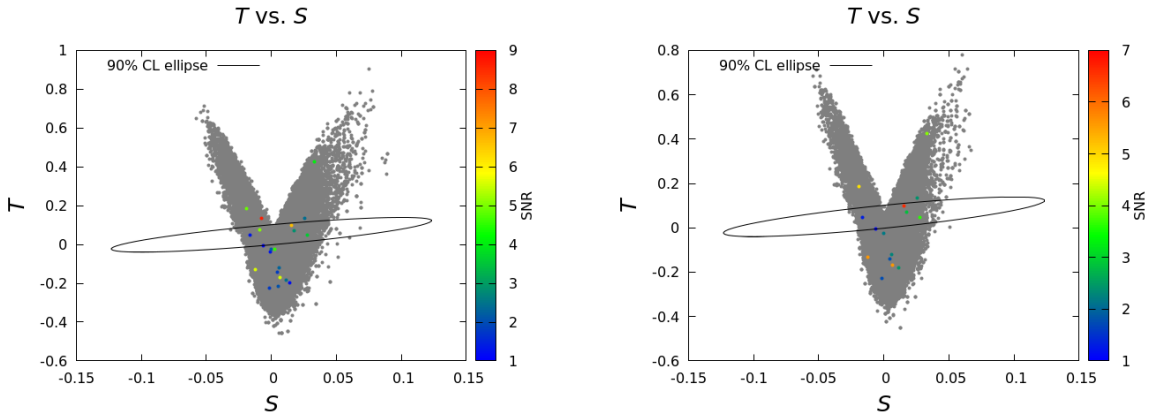

(a) Without HB/HS constraints.

(b) With HB/HS constraints.

Figure 5: The oblique parameters S and T along with the ST ellipsis $\mathcal{E}_{ST}$ for two cases: a) Without HB/HS constraints and b) With HB/HS constraints. SNR computed at $v_w = 1$.

While the statistics is not very high, we note in figure 5b that it is possible to find points that satisfy all constraints and which would likely correspond to a detectable GW wave signal in the LISA detector (by having an SNR significantly larger than 1). For example, we can identify a benchmark point with an SNR of about 6.6, computed at $v_w = 1$. As discussed in section 2.5, the wall speed v_w can in principle be calculated, but we treat it as "free" parameter for simplicity. Taking $v_w = 1$ for the SNR calculation gives the most conservative estimate, while taking $v_w = v_{\rm CJ}$ gives the most optimistic estimate. For the benchmark point in question, the SNR value at $v_w = v_{\rm CJ}$ is around 21.6. Unless otherwise stated, henceforth we will always calculate the SNR at $v_w = 1$. In figure 6, we show the GW power spectra (c.f. equation 2.68) for the benchmark point at $v_w = 1$ and $v_w = v_{\rm CJ}$, respectively, along with the LISA sensitivity curve. The only difference between the spectra at $v_w = 1$ and $v_w = v_{\rm CJ}$ is the peak amplitude.

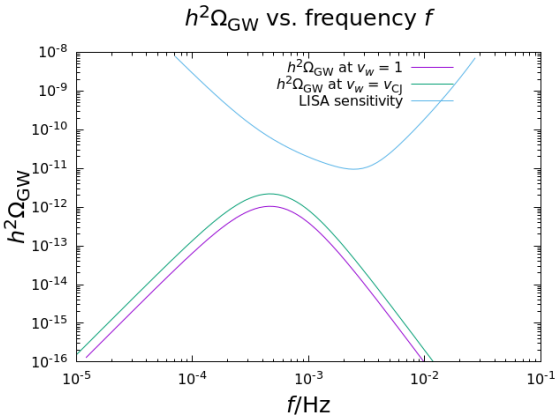

Figure 6: GW spectrum for a benchmark point.

A nice way to illustrate the power spectra for many points is by plotting the peak amplitude $(h^2\Omega_{\rm GW})_{\rm peak}$ vs. the peak frequency $f_{\rm peak}$ (as is done e.g. in [75]). This is done in figure 7 below, where we also include the PISCs (c.f. section 2.5) for the LISA, BBO and DECIGO detectors, along with the SNR in color code. Note that the sensitivity curves are terminated at the ends of the frequency range for the respective detector. In this plot, a point is observable by a specific detector if it lies at or above the PISC of the detector. Indeed, the four points with high SNR (as calculated for LISA) lie above the PISC for LISA; however, they appear to be outside the frequency range of BBO and DECIGO.

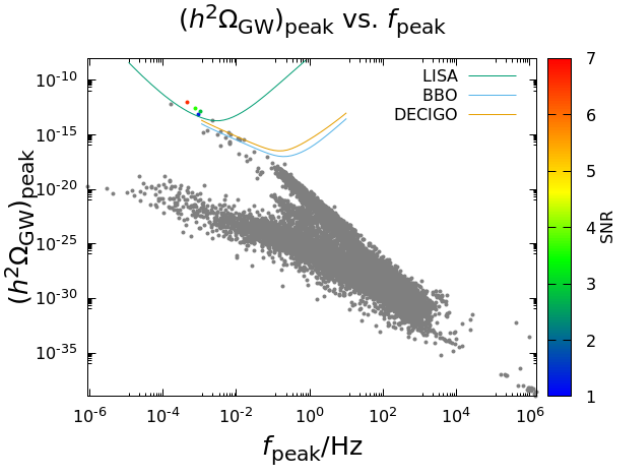

Figure 7: GW peak amplitude $(h^2\Omega_{\rm GW})_{\rm peak}$ vs. peak frequency $f_{\rm peak}$ in E2HDM.

We are interested in understanding when a 2HDM would give rise to a SFOEWPT that would be observable through the GWB. Let us therefore consider how the strength of the GWB correlates with various parameters. First of all, let us consider how the strength of the GWB correlates with the strength α, inverse duration β/H and order parameter $\Delta v_n/T_n$ of the phase transition. Figure 8 shows the peak amplitude $(h^2\Omega_{\rm GW})_{\rm peak}$ vs. α, β/H and $\Delta v_n/T_n$. We see that the peak amplitude correlates with large values of α and small values of β/H. The correlation with $\Delta v_n/T_n$ is not as clear, and α appears to be a better indicator of the strength of the GW signal.

It would also interesting to see how the peak amplitude $(h^2\Omega_{\rm GW})_{\rm peak}$ correlates with various parameters of the 2HDM. Figure 9 shows $(h^2\Omega_{\rm GW})_{\rm peak}$ vs. the Higgs boson masses m_h, m_H, m_A and $m_{H^\pm}$, $s_{\beta-\alpha}$ and t_β. From these figures, it is not possible to discern any clear correlation between the peak amplitude and the parameters considered. More statistics in the region of high $(h^2\Omega_{\rm GW})_{\rm peak}$ might reveal a different picture. Note that the feature where points are absent near $t_\beta = 1$ in figure 9f is likely caused by issues with numerical degeneracy in `2HDMC` for this region [76].

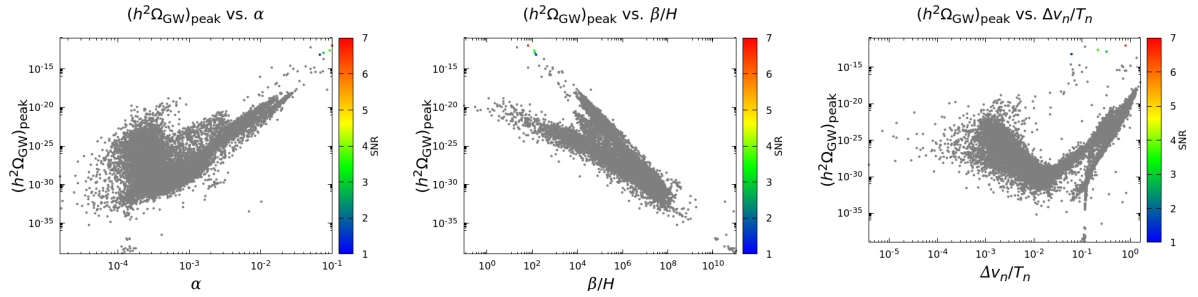

(a) α (b) β/H (c) $\Delta v_n/T_n$

Figure 8: GWB peak amplitude $(h^2\Omega_{\rm GW})_{\rm peak}$ vs. a) α, b) β/H and c) $\Delta v_n/T_n$ in E2HDM.

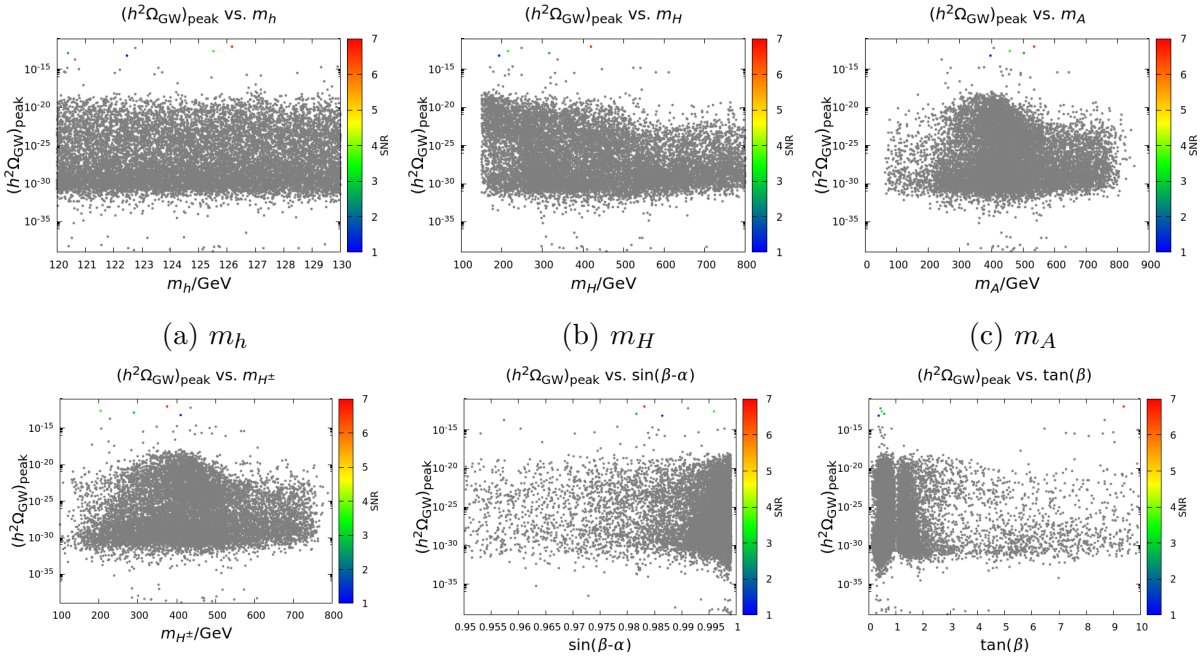

(a) m_h (b) m_H (c) m_A

(d) $m_{H^\pm}$ (e) $s_{\beta-\alpha}$ (f) t_β

Figure 9: GWB peak amplitude $(h^2\Omega_{\rm GW})_{\rm peak}$ vs. masses of the Higgs bosons, $s_{\beta-\alpha}$ and t_β in E2HDM.

In a similar spirit, figure 10 shows the peak amplitude $(h^2\Omega_{\rm GW})_{\rm peak}$ vs. the normalized Yukawa couplings ρ_f/κ_f, $f = t, b, \tau$. Again, it is not possible to discern any clear correlations.

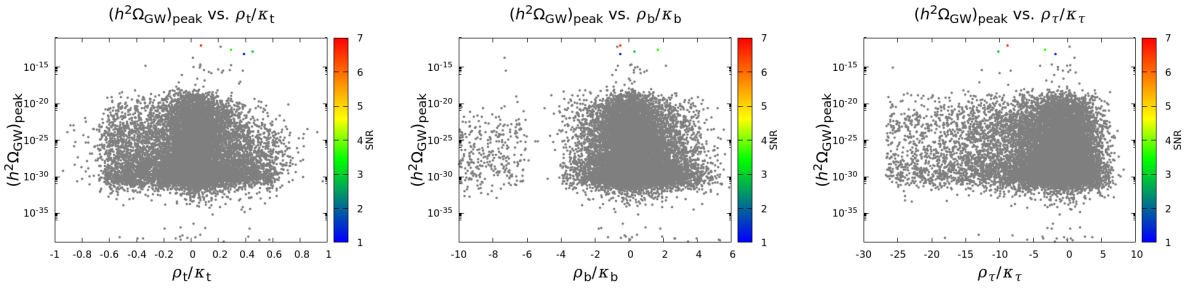

(a) ρ_t/κ_t (b) ρ_b/κ_b (c) ρ_τ/κ_τ

Figure 10: GWB peak amplitude $(h^2\Omega_{\rm GW})_{\rm peak}$ vs. normalized Yukawa couplings in E2HDM.

An interesting phenomenological signal of the Higgs sector is the self interaction of the light Higgs boson [77]. In figure 11 below we show the peak amplitude $(h^2\Omega_{\rm GW})_{\rm peak}$ vs. $|\lambda_{hhh}|$ and $|\lambda_{hhhh}|$, and in figure 12 we show α vs. $|\lambda_{hhh}|$ and $|\lambda_{hhhh}|$. In the discussion of phase transitions in the SM in 2.4.2 we saw, qualitatively, that for a (strongly) FOPT we cannot have a large quartic coupling $\lambda(T)$ compared to the cubic coupling E (c.f. equation 2.43). On the basis of this, we might have expected a negative correlation between $(h^2\Omega_{\rm GW})_{\rm peak}$ and $|\lambda_{hhhh}|$ in figure 11b, between α and $|\lambda_{hhhh}|$ in figure 12b. However, such a correlation is not present.

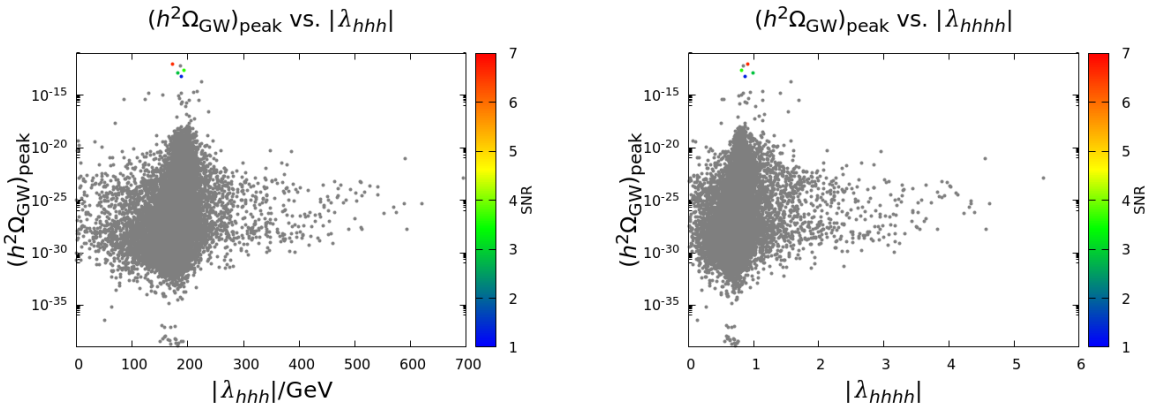

(a) $|\lambda_{hhh}|$ (b) $|\lambda_{hhhh}|$

Figure 11: $(h^2\Omega_{\rm GW})_{\rm peak}$ vs. $|\lambda_{hhh}|$ and $|\lambda_{hhhh}|$ in E2HDM.

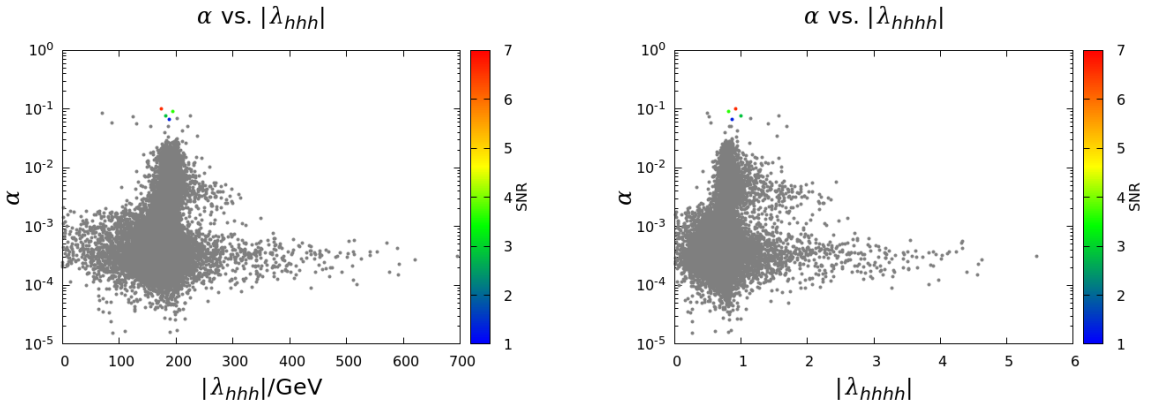

(a) $|\lambda_{hhh}|$ (b) $|\lambda_{hhhh}|$

Figure 12: α vs. $|\lambda_{hhh}|$ and $|\lambda_{hhhh}|$ in E2HDM.

To conclude this section, we have seen that it is possible to realize SFOPTs in the E2HDM. For a few benchmark points, the phase transition is strong enough and of short enough duration, to produce a GWB signal that would be observable by the LISA detector. This shows that if LISA, or another future GW detector, *does* in fact detect a GWB signal that can be attributed to a SFOPT in the early universe, the E2HDM would be a viable model to explain such signals.

4.2 C2HDM

Since, in the C2HDM, the various 2HDM parameters are calculated from the composite dynamics, it is natural to consider how they are distributed vs. the compositeness scale f.

In figure 13 below, we show the potential parameters vs. the compositeness scale f. Note that, as mentioned in section 2.3, we have $\lambda_6 = \lambda_7 = (5/3)m_{12}^2$. To highlight the influence of the experimental constraints due to `HB/HS` and the ST-ellipse, we show both the points with no constraints imposed (grey) and with the experimental constraints imposed (green) [16]. Notably, we get negative values of λ_1 and λ_2. As discussed in section 3.3.1, we would not accept such values in the elementary case due to the requirement of positivity/stability of the potential. In figure 14 we show the Higgs vev v, as well as the calculated SM value of the vev $v_{\text{SM}}^{\text{calc}}$ that is implied from equation 2.23. Both v and $v_{\text{SM}}^{\text{calc}}$ are constrained by the condition that $v_{\text{SM}}^{\text{calc}}$ differs by less than 2% from v_{SM}, where $v_{\text{SM}} = 246.22$ GeV.

[16] In total, there were around $3.4 \cdot 10^4$ points. Of these, around $5.5 \cdot 10^3$ points passed the `HB/HS` constraints, and around $3.7 \cdot 10^4$ points passed the constraints from `HB/HS` and the ST-ellipse.

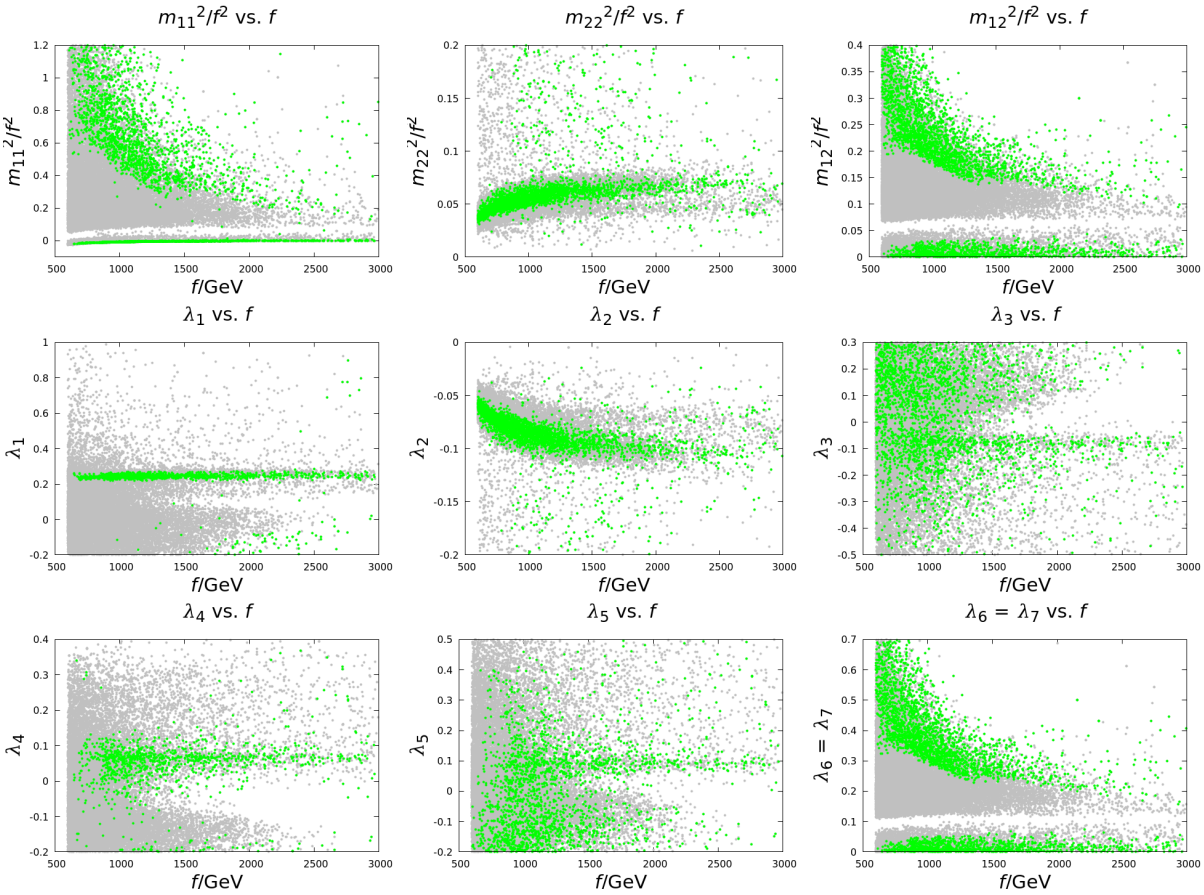

Figure 13: Parameters of the Higgs potential in C2HDM vs. the composite scale parameter f. Grey: no experimental constraints imposed. Green: constraints from `HB/HS` and the ST-ellipse imposed.

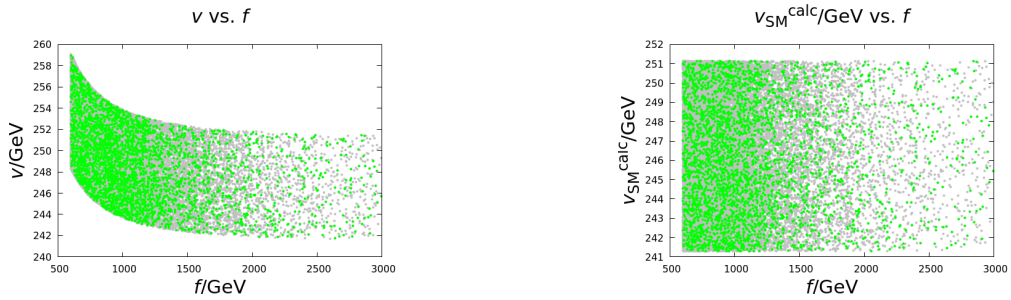

Figure 14: The vevs v and $v_{\rm SM}^{\rm calc}$ in C2HDM. Grey: no experimental constraints imposed. Green: constraints from `HB/HS` and the ST-ellipse imposed.

Further, in figure 15 we show the masses of the Higgs bosons, as well as t_β and $s_{\beta-\alpha}$. Notably, there is a band of missing points around $t_\beta = 1$ and, as discussed in section 4.1, this likely has to do with issues of numerical degeneracy in `2HDMC` in this region.

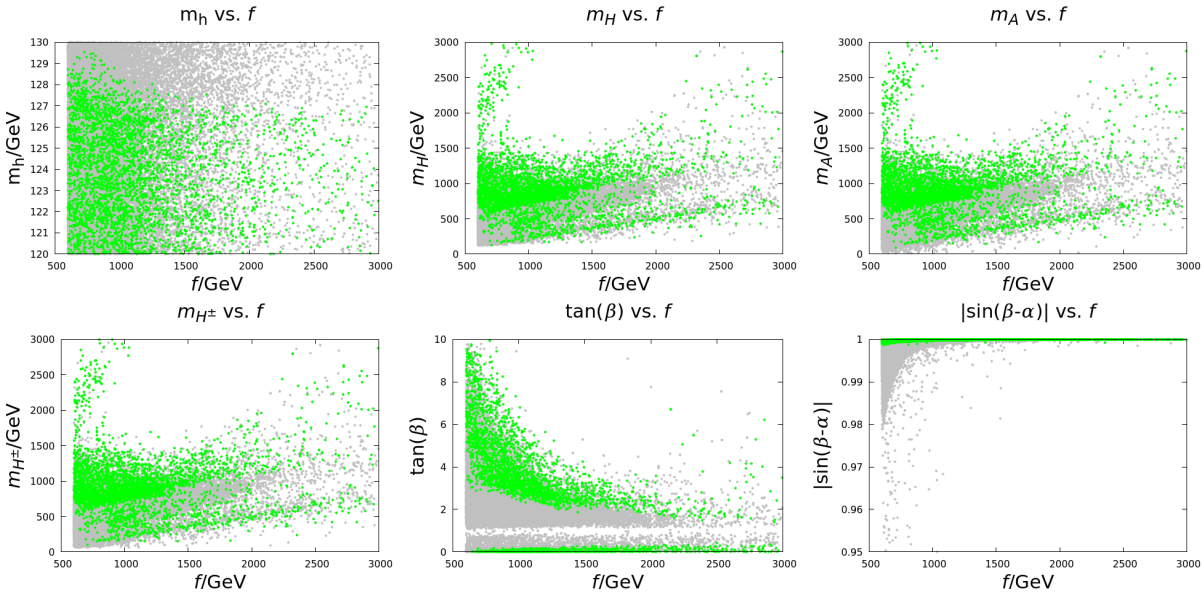

Figure 15: Masses of the Higgs bosons, t_β as well as $s_{\beta-\alpha}$ in C2HDM. Grey: no experimental constraints imposed. Green: constraints from `HB/HS` and the ST-ellipse imposed.

As an illustration of the compositeness corrections, in figure 16 we show the Higgs self couplings $|\lambda_{hhh}|$ and $|\lambda_{hhhh}|$ vs. the compositeness scale parameter f. The self couplings receive compositeness corrections, and in the limit $f \to \infty$ they approach the values in E2HDM, according to table 3. Since the alignment limit $|\sin(\beta-\alpha)| \to 1$ is approximately realized, these values are fairly close to SM values according to equation 2.7.

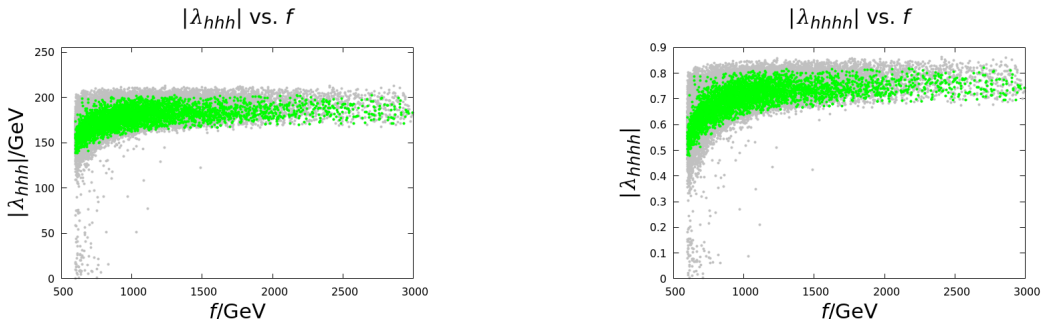

Figure 16: The trilinear and quartic self Higgs couplings $|\lambda_{hhh}|$ and $|\lambda_{hhhh}|$ in C2HDM. Green: constraints from `HB/HS` and the ST-ellipse imposed.

Finally, let us consider phase transitions in C2HDM. Figure 17 shows the GW peak amplitude $(h^2\Omega_{\rm GW})_{\rm peak}$ vs. peak frequency $f_{\rm peak}$, along with the PISCs for LISA, BBO and DECIGO. In figure 18, we consider the dependence of $(h^2\Omega_{\rm GW})_{\rm peak}$, α, β/H and $\Delta v_n/T_n$ on the compositeness scale parameter f. Note, in these figures, that there is no SNR above 1. Despite this, we keep the colour code to keep the plots consistent with those in section

4.1. It appears that large values of $(h^2\Omega_{\rm GW})_{\rm peak}$ correlates with low values of f. Consistent with this trend, large values of α and small values of β/H correlate with small values of f. For the order parameter $\Delta v_n/T_n$, the correlation with f is not very clear.

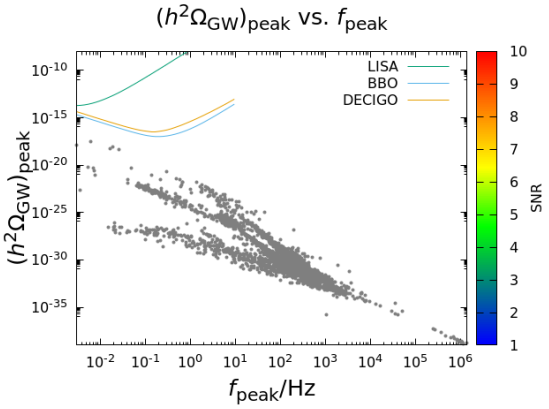

Figure 17: GW peak amplitude $(h^2\Omega_{\rm GW})_{\rm peak}$ vs. peak frequency $f_{\rm peak}$.

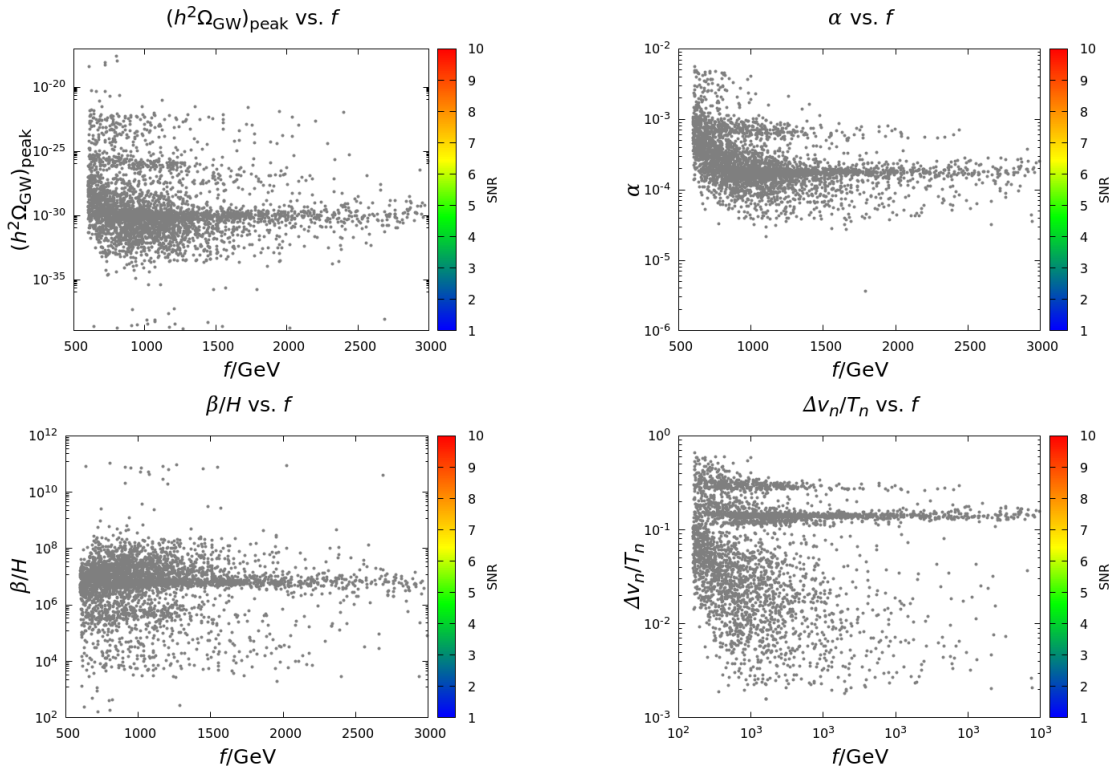

Figure 18: $(h^2\Omega_{\rm GW})_{\rm peak}$, α, β/H and $\Delta v_n/T_n$ vs. the compositeness scale f in C2HDM.

5 Conclusion

In this project, we have considered some phenomenological aspects of 2HDMs in two forms: elementary and composite. Elementary and composite 2HDMs are natural extensions of the minimal Higgs sector in the SM, and can potentially address some of the questions which are unanswered by the SM. Our focus has been on aspects of the phase transition connected with electroweak symmetry breaking in the early universe.

As is well known, in the SM this phase transition cannot be strong enough to explain the observed baryon asymmetry of the universe. On the other hand, in 2HDMs, a strong enough phase transition *can* be realized to address the problem of the baryon asymmetry. An interesting signal of such a phase transition could appear in the form of a contribution to the gravitational wave background of the universe, to be probed by future gravitational wave detectors.

Our approach in this project has been to mainly use collider phenomenology as a way to restrict the class of possible realizations of elementary and composite 2HDMs, and to analyze admissible realizations with respect to the phase transition properties and gravitational wave signals. We find that first order phase transitions can be realized in both elementary and composite models, and that these transitions could potentially be strong enough to generate an observable gravitational wave signal.

The investigation of phase transitions in the particular composite 2HDM considered is, to the best knowledege of the author, new. One potentially interesting finding is an apparent correlation between the strength of the phase transition and small values of the compositeness energy scale. This suggests an avenue for further investigations into the correlation between phase transition parameters and underlying properties of the composite model.

Acknowledgments

In this section I wish to thank all those who have, in one form or another, been helpful to me during the course of my work on this project. First of all I would like to thank my supervisors, Johan Rathsman and Roman Pasechnik, for their guidance throughout the project and for their helpful comments and suggestions. Jonas Wittbrodt has kindly answered numerous questions regarding `HiggsBounds`, `HiggsSignals` and `BSMPT`. António Morais has provided useful suggestions regarding the gravitational wave part of the project, particularly the sensitivity curves for the detectors. Christian Bierlich and Mattias Ohlsson have been helpful in getting the simulations to run on the department computers. Stefania De Curtis, Luigi Delle Rose and Stefano Moretti clarified various aspects of their composite 2HDM. In particular I thank Luigi Delle Rose for feedback regarding the implementation. I also thank Jens Erler and Ayres Freitas for help with the ST-ellipse. Last, but certainly not least, I want to thank my mother for her support.

A Details on the elementary two-Higgs doublet model

A.1 Interactions between gauge bosons and Higgs bosons

In this appendix, we provide the derivation of the couplings between gauge and Higgs bosons in E2HDM. The couplings are also given in tables 1 and 2 above. Let $\gamma = \beta - \alpha$ so that $\alpha = \beta - \gamma$, $\cos\alpha = \cos\beta\cos\gamma + \sin\beta\sin\gamma$ and $\sin\alpha = \sin\beta\cos\gamma - \cos\beta\sin\gamma$. In the Higgs basis, with $\beta = 0$, we have

$$\Phi_1 = \frac{1}{\sqrt{2}}\begin{pmatrix}\sqrt{2}G^+\\ v + hs_\gamma + Hc_\gamma + iG^0\end{pmatrix},\ \Phi_2 = \frac{1}{\sqrt{2}}\begin{pmatrix}\sqrt{2}H^+\\ hc_\gamma - Hs_\gamma + iA\end{pmatrix}$$

Further, we can perform a gauge transformation to suppress the Goldstone modes, thus going to unitarity gauge where we expand according to

$$\Phi_1 = \frac{1}{\sqrt{2}}\begin{pmatrix}0\\ v + hs_\gamma + Hc_\gamma\end{pmatrix},\ \Phi_2 = \frac{1}{\sqrt{2}}\begin{pmatrix}\sqrt{2}H^+\\ hc_\gamma - Hs_\gamma + iA\end{pmatrix}$$

With $Y_1 = Y_2 = 1$, $g' = gt_W$, $e = gs_W$, $B_\mu = c_W A_\mu - s_W Z_\mu$, $W^3_\mu = s_W A_\mu + c_W Z_\mu$ and $W^\pm_\mu = (-W^1_\mu \pm iW^2_\mu)/\sqrt{2}$, where $c_W = \cos\theta_W$, $s_W = \sin\theta_W$ and $t_W = \tan\theta_W$, we get

$$D_\mu\Phi_1 = \frac{1}{\sqrt{2}}\begin{pmatrix} ig\frac{\sqrt{2}}{2}W^+_\mu(v + hs_\gamma + Hc_\gamma)\\ \\ \partial_\mu(hs_\gamma + Hc_\gamma) + ig\frac{1}{2c_W}Z_\mu(v + hs_\gamma + Hc_\gamma)\end{pmatrix}$$

$$D_\mu\Phi_2 = \frac{1}{\sqrt{2}}\begin{pmatrix}\sqrt{2}\partial_\mu H^+ - ig\frac{\sqrt{2}}{2}\frac{c_{2W}}{c_W}Z_\mu H^+ - ie\sqrt{2}A_\mu H^+ + ig\frac{\sqrt{2}}{2}W^+_\mu(hc_\gamma - Hs_\gamma + iA)\\ \\ \partial_\mu(hc_\gamma - Hs_\gamma) + i\partial_\mu A + igW^-_\mu H^+ + ig\frac{1}{2c_W}Z_\mu(hc_\gamma - Hs_\gamma + iA)\end{pmatrix}$$

In the kinetic Lagrangian the terms $(\frac{gv}{2})^2 W^+_\mu W^{\mu-}$ and $\frac{1}{2}(\frac{gv}{2c_W})^2 Z_\mu Z^\mu$ appear, from which the masses $m_W = \frac{gv}{2}$ and $m_Z = \frac{gv}{2c_W}$ can be identified. After some simplifications the kinetic Lagrangian becomes

$$\mathcal{L}_{\text{kin}} = \mathcal{L}_{\text{der}} + \mathcal{L}_{\text{mass}} + \mathcal{L}_{\text{VVH}} + \mathcal{L}_{\text{VHH}} + \mathcal{L}_{\text{VVHH}},$$

where

$$\begin{aligned}
\mathcal{L}_{\text{der}} &= \frac{1}{2}(\partial^\mu h)(\partial_\mu h) + \frac{1}{2}(\partial^\mu H)(\partial_\mu H) + \frac{1}{2}(\partial^\mu A)(\partial_\mu A) + (\partial^\mu H^-)(\partial_\mu H^+)\\
\mathcal{L}_{\text{mass}} &= m^2_W W^+_\mu W^{\mu-} + \frac{1}{2}m^2_Z Z_\mu Z^\mu\\
\mathcal{L}_{\text{VVH}} &= gm_W s_\gamma W^+_\mu W^{\mu-} h + gm_W c_\gamma W^+_\mu W^{\mu-} H + \frac{1}{2}\frac{gm_Z}{c_W}s_\gamma Z_\mu Z^\mu h + \frac{1}{2}\frac{gm_Z}{c_W}c_\gamma Z_\mu Z^\mu H
\end{aligned}$$

$$
\begin{aligned}
\mathcal{L}_{\text{VHH}} = &-\frac{ig}{2}c_\gamma W^{\mu+}H^-\overleftrightarrow{\partial}_\mu h + \frac{ig}{2}c_\gamma W^{\mu-}H^+\overleftrightarrow{\partial}_\mu h + \frac{ig}{2}s_\gamma W^{\mu+}H^-\overleftrightarrow{\partial}_\mu H \\
&- \frac{ig}{2}s_\gamma W^{\mu-}H^+\overleftrightarrow{\partial}_\mu H + \frac{g}{2}W^{\mu\pm}H^\mp\overleftrightarrow{\partial}_\mu A - \frac{g}{2c_W}c_\gamma Z^\mu A\overleftrightarrow{\partial}_\mu h \\
&+ \frac{g}{2c_W}s_\gamma Z^\mu A\overleftrightarrow{\partial}_\mu H + \frac{igc_{2W}}{2c_W}Z^\mu H^-\overleftrightarrow{\partial}_\mu H^+ + ieA^\mu H^-\overleftrightarrow{\partial}_\mu H^+ \\
\mathcal{L}_{\text{VVHH}} = &\frac{1}{2}\frac{g^2}{2}W^+_\mu W^{\mu-}hh + \frac{1}{2}\frac{g^2}{2}W^+_\mu W^{\mu-}HH + \frac{1}{2}\frac{g^2}{2}W^+_\mu W^{\mu-}AA + \frac{g^2}{4}W^+_\mu W^{\mu-}H^+H^- \\
&+ \frac{1}{4}\frac{g^2}{2c_W^2}Z_\mu Z^\mu hh + \frac{1}{4}\frac{g^2}{2c_W^2}Z_\mu Z^\mu HH + \frac{1}{4}\frac{g^2}{2c_W^2}Z_\mu Z^\mu AA + \frac{1}{2}\frac{g^2c_{2W}^2}{2c_W^2}Z_\mu Z^\mu H^+H^- \\
&+ \frac{g^2s_W^2}{2c_W}c_\gamma W^\pm_\mu Z^\mu hH^\mp - \frac{g^2s_W^2}{2c_W}s_\gamma W^\pm_\mu Z^\mu HH^\mp - \frac{ge}{2}c_\gamma W^\pm_\mu A^\mu hH^\mp \\
&+ \frac{ge}{2}s_\gamma W^\pm_\mu A^\mu HH^\mp + \frac{gec_{2W}}{c_W}Z_\mu A^\mu H^+H^- + \frac{1}{2}2e^2A_\mu A^\mu H^+H^-
\end{aligned}
$$

The operator $\overleftrightarrow{\partial}_\mu$ is defined by $X\overleftrightarrow{\partial}_\mu Y = X(\partial_\mu Y) - Y(\partial_\mu X)$.

B Details on the composite two-Higgs doublet model

B.1 Derivation of the expression for the top mass

As discussed in section 3.5, one of the constraints that is used for simulations in C2HDM is to have a top mass in an acceptable range around the measured value. Below, we sketch the derivation of the top mass in the composite model, since the full expression is not explpicitly given in [19]. Consider the effective Lagrangian in equation 3.11 in [19], i.e.

$$
\begin{aligned}
\mathcal{L}^{\text{fermion}}_{\text{Composite}} = &(\bar{q}^{\mathbf{6}}_L)_t \not{k}[\tilde{\Pi}^{q_t}_0(k^2) + \tilde{\Pi}^{q_t}_1(k^2)\Sigma + \tilde{\Pi}^{q_t}_2(k^2)\Sigma^2](q^{\mathbf{6}}_R)_t \\
&+ \bar{t}^{\mathbf{6}}_L \not{k}[\tilde{\Pi}^t_0(k^2) + \tilde{\Pi}^t_1(k^2)\Sigma + \tilde{\Pi}^t_2(k^2)\Sigma^2]t^{\mathbf{6}}_R \\
&+ (\bar{q}^{\mathbf{6}}_L)_t[\tilde{M}^t_0(k^2) + \tilde{M}^t_1(k^2)\Sigma + \tilde{M}^t_2(k^2)\Sigma^2]t^{\mathbf{6}}_R + (t \to b, \tau) + \text{ h.c.}
\end{aligned} \tag{B.1}
$$

The Σ field is given by $\Sigma = U_1\Sigma_2U_1^T = U_1U_2\Sigma_0U_2^TU_1^T$. Following earlier calculations in the gauge sector we can write down the expression for Σ to first order in the Higgs fields. We find that

$$
\Sigma = \sqrt{2}i\left(T_s + \frac{i}{f}[\Pi, T_s] + ...\right) = \sqrt{2}i\left(T_s + \frac{i}{f}\sqrt{2}h^{\hat{a}}_\alpha[\hat{T}^{\hat{a}}_\alpha, T_s] + ...\right).
$$

For the term $\tilde{M}^t_1(0)\Sigma$ the relevant term in the expression for Σ is

$$
\tilde{M}^t_1(0)\Sigma : \Sigma \to \sqrt{2}i\frac{i}{f}\sqrt{2}h^{\hat{a}}_\alpha[\hat{T}^{\hat{a}}_\alpha, T_s] = \frac{1}{f}\begin{pmatrix} 0_{4\times4} & -\boldsymbol{h}_2 & \boldsymbol{h}_1 \\ \boldsymbol{h}_2^T & 0 & 0 \\ -\boldsymbol{h}_2^T & 0 & 0 \end{pmatrix}, \tag{B.2}
$$

where we introduced the notation $\boldsymbol{h}_i = (h_i^1, h_i^2, h_i^3, h_i^4)^T$, $i = 1, 2$. For the term $\tilde{M}_2^t(0)\Sigma^2$ the relevant term for Σ^2 is

$$\tilde{M}_2^t(0)\Sigma^2 : \Sigma^2 \to (\sqrt{2}i)^2\sqrt{2}h_\alpha^{\hat{a}}\frac{i}{f}\left(T_S[\hat{T}_\alpha^{\hat{a}}, T_s] + [\hat{T}_\alpha^{\hat{a}}, T_s]T_S\right) = \frac{1}{f}\begin{pmatrix} 0_{4\times4} & -\boldsymbol{h}_2 & \boldsymbol{h}_1 \\ \boldsymbol{h}_2^T & 0 & 0 \\ -\boldsymbol{h}_2^T & 0 & 0 \end{pmatrix}. \quad \text{(B.3)}$$

The relevant spurion vevs are given by (see equation 3.9 in [19])

$$\langle\Upsilon_L^t\rangle = \frac{1}{\sqrt{2}}\begin{pmatrix} 0 & 0 & 1 & i & 0 & 0 \\ 1 & -i & 0 & 0 & 0 & 0 \end{pmatrix},\ \langle\Upsilon_R^t\rangle = \frac{1}{\sqrt{2}}\begin{pmatrix} 0 & 0 & 0 & 0 & \cos\theta_t & i\sin\theta_t. \end{pmatrix}$$

However, $\mathcal{CP}$-conservation requires that $\theta_t = 0$, so we have

$$\langle\Upsilon_L^t\rangle = \frac{1}{\sqrt{2}}\begin{pmatrix} 0 & 0 & 1 & i & 0 & 0 \\ 1 & -i & 0 & 0 & 0 & 0 \end{pmatrix},\ \langle\Upsilon_R^t\rangle = \frac{1}{\sqrt{2}}\begin{pmatrix} 0 & 0 & 0 & 0 & 1 & 0 \end{pmatrix}.$$

To proceed, we note that the Higgs doublets are given by

$$\frac{1}{\sqrt{2}}\begin{pmatrix} h_1^2 + ih_1^1 \\ h_1^4 - ih_1^3 \end{pmatrix} = \frac{1}{\sqrt{2}}\begin{pmatrix} \sqrt{2}\varphi_1^+ \\ v\cos\beta + \eta_1 + i\chi_1 \end{pmatrix}$$
$$\frac{1}{\sqrt{2}}\begin{pmatrix} h_2^2 + ih_2^1 \\ h_2^4 - ih_2^3 \end{pmatrix} = \frac{1}{\sqrt{2}}\begin{pmatrix} \sqrt{2}\varphi_2^+ \\ v\sin\beta + \eta_2 + i\chi_2 \end{pmatrix}$$

We find that

$$\langle\Upsilon_L^t\rangle\Sigma\langle\Upsilon_R^t\rangle^T = \frac{1}{\sqrt{2}f}\begin{pmatrix} -(h_2^3 + ih_2^4) \\ -(h_2^1 - ih_2^2) \end{pmatrix} = \frac{1}{\sqrt{2}f}\begin{pmatrix} -i(v\sin\beta + \eta_2) + \chi_2 \\ i\sqrt{2}\varphi_2^+ \end{pmatrix}$$

and similarly

$$\langle\Upsilon_L^t\rangle\Sigma^2\langle\Upsilon_R^t\rangle^T = \frac{1}{\sqrt{2}f}\begin{pmatrix} -(h_1^3 + ih_1^4) \\ -(h_1^1 - ih_1^2) \end{pmatrix} = \frac{1}{\sqrt{2}f}\begin{pmatrix} -i(v\cos\beta + \eta_1) + \chi_1 \\ i\sqrt{2}\varphi_1^+ \end{pmatrix}$$

The mass term is extracted from equation B.1 by keeping the terms with the vevs that go with $\bar{t}_L t_R$ and dividing by $-i\sqrt{\tilde{\Pi}_0^{q_t}(0)\tilde{\Pi}_0^t(0)}$ to get

$$\frac{v}{\sqrt{2}f}\left[\sin\beta M_1^t(0) + \cos\beta M_2^t(0)\right]\bar{t}_L t_R$$

One has $M_1^t(0) = Y_1 M^t(0)$ and $M_2^t(0) = Y_2 M^t(0)$, where

$$M^t(0) = \frac{m_{\Psi_1}m_{\Psi_2}\Delta_L\Delta_R}{\sqrt{m_{\Psi_1}^2m_{\Psi_2}^2 + (m_{\Psi_2}^2 + m_{\Psi_{12}}^2)\Delta_L^2}\sqrt{m_{\Psi_1}^2m_{\Psi_2}^2 + (m_{\Psi_1}^2 + Y^2)\Delta_R^2}}.$$

Thus, we get the following expression for the top mass:

$$m_t = \frac{v}{\sqrt{2}}\frac{m_{\Psi_1}m_{\Psi_2}\Delta_L\Delta_R}{\sqrt{m_{\Psi_1}^2m_{\Psi_2}^2 + (m_{\Psi_2}^2 + m_{\Psi_{12}}^2)\Delta_L^2}\sqrt{m_{\Psi_1}^2m_{\Psi_2}^2 + (m_{\Psi_1}^2 + Y^2)\Delta_R^2}}\frac{Y_1 s_\beta + Y_2 c_\beta}{f}. \quad \text{(B.4)}$$

B.2 Calculation of the parameters of the Higgs potential

The expressions for the parameters of the Higgs potential in terms of the composite parameters are derived in [19]. All integrals to be computed have the form $-i\int \frac{d^4k}{(2\pi)^4} g(k^2)$, for some function g. By Wick rotation, we have $-i\int \frac{d^4k}{(2\pi)^4} g(k^2) = \frac{f^4}{16\pi^2}\int_0^\infty x g(-f^2 x)dx$, where $f > 0$ is a scale factor with dimension of energy, taken to be the compositeness scale of the model. Following equation 4.2 in [19], the parameters of the potential are then given by

$$\begin{aligned}
\frac{m_{ij}^2}{f^2} &= \frac{-i}{f^6}\int \frac{d^4k}{(2\pi)^4}\left[\frac{3}{2}(m_{ij}^G)^2[k^2] - 6(m_{ij}^F)^2[k^2]\right] = \\
&= \frac{1}{16\pi^2}\int_0^\infty x\left[\frac{3}{2}\frac{(m_{ij}^G)^2[-f^2x]}{f^2} - 6\frac{(m_{ij}^F)^2[-f^2x]}{f^2}\right]dx \\
\lambda_j &= \frac{-i}{f^4}\int \frac{d^4k}{(2\pi)^4}\left[\frac{3}{2}\lambda_j^G[k^2] - 6\lambda_j^F[k^2]\right] = \\
&= \frac{1}{16\pi^2}\int_0^\infty x\left[\frac{3}{2}\lambda_j^G[-f^2x] - 6\lambda_j^F[-f^2x]\right]dx
\end{aligned}$$

These integrals can be computed from the expressions given in equations 4.3, 4.4 and appendix B in [19]. We have done so and implemented the expressions in the utility program `CompUtil`, as described in section 3.5. In the notation of [19], for the gauge part, we need the following integrals

$$\begin{aligned}
I_W &:= \frac{-i}{f^4}\int \frac{d^4k}{(2\pi)^4}\bar{\Pi}_W = \frac{1}{16\pi^2}\int_0^\infty x\bar{\Pi}_W[-f^2x]dx \\
I_B &:= \frac{-i}{f^4}\int \frac{d^4k}{(2\pi)^4}\bar{\Pi}_B = \frac{1}{16\pi^2}\int_0^\infty x\bar{\Pi}_B[-f^2x]dx \\
I_{WW} &:= \frac{-i}{f^2}\int \frac{d^4k}{(2\pi)^4}\bar{\Pi}_W = \frac{1}{16\pi^2}\int_{(\mu/f)^2}^\infty x\bar{\Pi}_W[-f^2x]^2dx \\
I_{WB} &:= \frac{-i}{f^4}\int \frac{d^4k}{(2\pi)^4}\bar{\Pi}_W = \frac{1}{16\pi^2}\int_{(\mu/f)^2}^\infty x\bar{\Pi}_W[-f^2x]\bar{\Pi}_B[-f^2x]dx \\
I_{BB} &:= \frac{-i}{f^4}\int \frac{d^4k}{(2\pi)^4}\bar{\Pi}_W = \frac{1}{16\pi^2}\int_{(\mu/f)^2}^\infty x\bar{\Pi}_B[-f^2x]^2dx
\end{aligned}$$

and for the fermionic part we need the following integrals

$$
\begin{aligned}
J_{\Pi_2^{q_t}} &:= \frac{-i}{f^4}\int \frac{d^4k}{(2\pi)^4}\Pi_2^{q_t} = \frac{1}{16\pi^2}\int_0^\infty x\Pi_2^{q_t}[-f^2x]dx \\
J_{(\Pi_2^{q_t})^2} &:= \frac{-i}{f^4}\int \frac{d^4k}{(2\pi)^4}(\Pi_2^{q_t})^2 = \frac{1}{16\pi^2}\int_0^\infty x(\Pi_2^{q_t}[-f^2x])^2dx \\
J_{\Pi_2^{t}} &:= \frac{-i}{f^4}\int \frac{d^4k}{(2\pi)^4}\Pi_2^{t} = \frac{1}{16\pi^2}\int_0^\infty x\Pi_2^{t}[-f^2x]dx \\
J_{(\Pi_2^{t})^2} &:= \frac{-i}{f^4}\int \frac{d^4k}{(2\pi)^4}(\Pi_2^{t})^2 = \frac{1}{16\pi^2}\int_0^\infty x(\Pi_2^{t}[-f^2x])^2dx \\
J_{(M_1^t)^2} &:= \frac{-i}{f^4}\int \frac{d^4k}{(2\pi)^4}\frac{(M_1^t)^2}{k^2} = -\frac{1}{16\pi^2}\int_0^\infty (M_1^t[-f^2x])^2dx \\
J_{M_1^tM_2^t} &:= \frac{-i}{f^4}\int \frac{d^4k}{(2\pi)^4}\frac{M_1^tM_2^t}{k^2} = -\frac{1}{16\pi^2}\int_0^\infty M_1^t[-f^2x]M_2^t[-f^2x]dx \\
J_{(M_2^t)^2} &:= \frac{-i}{f^4}\int \frac{d^4k}{(2\pi)^4}\frac{(M_2^t)^2}{k^2} = -\frac{1}{16\pi^2}\int_0^\infty (M_2^t[-f^2x])^2dx.
\end{aligned}
$$

It is found that I_{WW}, I_{WB} and I_{BB} are logarithmically divergent in the lower limit. We introduce an infrared momentum cutoff to regulate this, and in the calculations, we put $\mu = m_W = 80$ GeV.

C Thermal mass corrections in 2HDM

In this appendix we present the expressions for the temperature and field dependent masses $m_i^2(\boldsymbol{\omega}, T)$ in 2HDM, for the setup presented in section 2.4.3. The expressions have been derived using the formulae in [34]. In the expressions below, we suppress the arguments $\boldsymbol{\omega}$ and T for simplicity.

First of all, from the Yukawa Lagrangian in equation 2.50, we read off the fermion masses:

$$
m_f^2 = \frac{1}{2}(a_f\omega_3 + b_f\omega_7)^2,\ \ f = t, b, \tau \tag{C.5}
$$

Note that the fermion masses receive no temperature corrections.

Next, let us consider the Higgs modes. Introduce the coefficients

$$
\begin{cases}
c_1 = \dfrac{1}{48}(12\lambda_1 + 8\lambda_3 + 4\lambda_4 + 3(3g^2 + g'^2)) \\
c_2 = \dfrac{1}{48}(12\lambda_2 + 8\lambda_3 + 4\lambda_4 + 3(3g^2 + g'^2)) \\
d_1 = \dfrac{1}{12}(3a_t^2 + 3a_b^2 + a_\tau^2) \\
d_2 = \dfrac{1}{12}(3a_tb_t + 3a_bb_b + a_\tau b_\tau) \\
d_3 = \dfrac{1}{12}(3b_t^2 + 3b_b^2 + b_\tau^2)
\end{cases}. \tag{C.6}
$$

For the neutral Higgs modes, we get a mass matrix $\mathcal{M}_N$

$$\mathcal{M}_N = \begin{pmatrix} \alpha_N & 0 & \beta_N & 0 \\ 0 & \gamma_N & 0 & \delta_N \\ \beta_N & 0 & \epsilon_N & 0 \\ 0 & \delta_N & 0 & \zeta_N \end{pmatrix}, \tag{C.7}$$

where the coefficients are given by

$$\begin{cases} \alpha_N = m_{11}^2 + \frac{3}{2}\lambda_1\omega_3^2 + \frac{1}{2}(\lambda_3+\lambda_4+\lambda_5)\omega_7^2 + 3\lambda_6\omega_3\omega_7 + (c_1+d_1)T^2 \\ \beta_N = -m_{12}^2 + \frac{3}{2}\lambda_6\omega_3^2 + \frac{3}{2}\lambda_7\omega_7^2 + \lambda_{345}\omega_3\omega_7 + d_2T^2 \\ \gamma_N = m_{11}^2 + \frac{1}{2}\lambda_1\omega_3^2 + \frac{1}{2}(\lambda_3+\lambda_4-\lambda_5)\omega_7^2 + \lambda_6\omega_3\omega_7 + (c_1+d_1)T^2 \\ \delta_N = -m_{12}^2 + \frac{1}{2}\lambda_6\omega_3^2 + \frac{1}{2}\lambda_7\omega_7^2 + \lambda_5\omega_3\omega_7 + d_2T^2 \\ \epsilon_N = m_{22}^2 + \frac{1}{2}(\lambda_3+\lambda_4+\lambda_5)\omega_3^2 + \frac{3}{2}\lambda_2\omega_7^2 + 3\lambda_7\omega_3\omega_7 + (c_2+d_3)T^2 \\ \zeta_N = m_{22}^2 + \frac{1}{2}(\lambda_3+\lambda_4-\lambda_5)\omega_3^2 + \frac{1}{2}\lambda_2\omega_7^2 + \lambda_7\omega_3\omega_7 + (c_2+d_3)T^2 \end{cases}. \tag{C.8}$$

The matrix $\mathcal{M}_N$ is readily diagonalized to yield the masses of the neutral Higgs modes:

$$\begin{cases} m_H^2 = \frac{1}{2}(\alpha_N+\epsilon_N) + \frac{1}{2}\sqrt{(\alpha_N-\epsilon_N)^2+4\beta_N^2} \\ m_h^2 = \frac{1}{2}(\alpha_N+\epsilon_N) - \frac{1}{2}\sqrt{(\alpha_N-\epsilon_N)^2+4\beta_N^2} \\ m_A^2 = \frac{1}{2}(\gamma_N+\zeta_N) + \frac{1}{2}\sqrt{(\gamma_N-\zeta_N)^2+4\delta_N^2} \\ m_{G^0}^2 = \frac{1}{2}(\gamma_N+\zeta_N) - \frac{1}{2}\sqrt{(\gamma_N-\zeta_N)^2+4\delta_N^2} \end{cases} \tag{C.9}$$

Similarly, for the charged Higgs modes we get a mass matrix $\mathcal{M}_C$

$$\mathcal{M}_C = \begin{pmatrix} \alpha_C & 0 & \beta_C & 0 \\ 0 & \alpha_C & 0 & \beta_C \\ \beta_C & 0 & \gamma_C & 0 \\ 0 & \beta_C & 0 & \gamma_C \end{pmatrix}, \tag{C.10}$$

where the coefficients are given by

$$\begin{cases} \alpha_C = m_{11}^2 + \frac{1}{2}\lambda_1\omega_3^2 + \frac{1}{2}\lambda_3\omega_7^2 + \lambda_6\omega_3\omega_7 + (c_1+d_1)T^2 \\ \beta_C = -m_{12}^2 + \frac{1}{2}(\lambda_4+\lambda_5)\omega_3\omega_7 + \frac{1}{2}\lambda_6\omega_3^2 + \frac{1}{2}\lambda_7\omega_7^2 + d_2T^2. \\ \gamma_C = m_{22}^2 + \frac{1}{2}\lambda_2\omega_7^2 + \frac{1}{2}\lambda_3\omega_3^2 + \lambda_7\omega_3\omega_7 + (c_2+d_3)T^2 \end{cases} \tag{C.11}$$

The matrix $\mathcal{M}_C$ can be easily diagonlized to yield the masses of the charged Higgs modes:

$$\begin{cases} m^2_{H^\pm} = \dfrac{1}{2}(\alpha_C + \gamma_C) + \dfrac{1}{2}\sqrt{(\alpha_C - \gamma_C)^2 + 4\beta_C^2} \\ m^2_{G^\pm} = \dfrac{1}{2}(\alpha_C + \gamma_C) - \dfrac{1}{2}\sqrt{(\alpha_C - \gamma_C)^2 + 4\beta_C^2} \end{cases}. \tag{C.12}$$

Note that while $\mathcal{M}_C$ is a 4×4 matrix we only get two distinct masses, since $H^\pm$ and $G^\pm$ are degenerate.

Finally, for the gauge bosons, we get the mass matrices $\mathcal{M}_{G_L}$ and $\mathcal{M}_{G_T}$, for longitudinal and transverse modes, respectively, given by

$$\mathcal{M}_{G_L} = \begin{pmatrix} \alpha_{G_L} & 0 & 0 & 0 \\ 0 & \alpha_{G_L} & 0 & 0 \\ 0 & 0 & \alpha_{G_L} & \gamma_{G_L} \\ 0 & 0 & \gamma_{G_L} & \beta_{G_L} \end{pmatrix}, \quad \mathcal{M}_{G_T} = \begin{pmatrix} \alpha_{G_T} & 0 & 0 & 0 \\ 0 & \alpha_{G_T} & 0 & 0 \\ 0 & 0 & \alpha_{G_T} & \gamma_{G_T} \\ 0 & 0 & \gamma_{G_T} & \beta_{G_T} \end{pmatrix} \tag{C.13}$$

where the coefficients are given by

$$\begin{cases} \alpha_{G_L} = \dfrac{1}{4}g^2(\omega_3^2 + \omega_7^2) + 2g^2T^2 \\ \beta_{G_L} = \dfrac{1}{4}g'^2(\omega_3^2 + \omega_7^2) + 2g'^2T^2, \\ \gamma_{G_L} = \dfrac{1}{4}gg'(\omega_3^2 + \omega_7^2) \end{cases} \quad \begin{cases} \alpha_{G_T} = \dfrac{1}{4}g^2(\omega_3^2 + \omega_7^2) \\ \beta_{G_T} = \dfrac{1}{4}g'^2(\omega_3^2 + \omega_7^2) \\ \gamma_{G_T} = \dfrac{1}{4}gg'(\omega_3^2 + \omega_7^2) \end{cases} \tag{C.14}$$

The mass matrices are easily diagonalized, yielding

$$\begin{cases} m^2_{W_L} = \alpha_{G_L} \\ m^2_{Z_L} = \dfrac{1}{2}(\alpha_{G_L} + \beta_{G_L}) + \dfrac{1}{2}\sqrt{(\alpha_{G_L} - \beta_{G_L})^2 + 4\gamma^2_{G_L}}, \\ m^2_{\gamma,L} = \dfrac{1}{2}(\alpha_{G_L} + \beta_{G_L}) - \dfrac{1}{2}\sqrt{(\alpha_{G_L} - \beta_{G_L})^2 + 4\gamma^2_{G_L}} \end{cases} \quad \begin{cases} m^2_{W_T} = \dfrac{1}{4}g^2(\omega_3^2 + \omega_7^2) \\ m^2_{Z_T} = \dfrac{1}{4}(g^2 + g'^2)(\omega_3^2 + \omega_7^2) \end{cases}. \tag{C.15}$$

Note that in the limit $T \to L$, and putting $\omega_3^2 + \omega_7^2 = v^2$, we recover the gauge boson masses introduced in connection with equation 2.6.

References

[1] T. W. Kibble, *The Standard Model of Particle Physics*, *Eur. Rev.* **23** (2015) 36 [arXiv:1412.4094v1 [physics.hist-ph]].

[2] S. Weinberg, *Essay: Half a century of the standard model*, *Phys. Rev. Lett.* **121** (2018) 220001.

[3] J. M. Butterworth, *The Standard Model: How far can it go and how can we tell?*, *Philos. Trans. R. Soc. A* **374** (2016) [arXiv:1601.02759v2 [hep-ex]].

[4] P. W. Higgs, *Broken symmetries and the masses of gauge bosons*, *Phys. Rev. Lett.* **13** (1964) 508.

[5] F. Abe *et al.* (CDF Collaboration), *Observation of Top Quark Production in $\bar{p}p$ Collisions with the Collider Detector at Fermilab*, *Phys. Rev. Lett.* **74** (1995) 2626.

[6] S. Abachi *et al.* (DØ Collaboration), *Observation of the Top Quark*, *Phys. Rev. Lett.* **74** (1995) 2632.

[7] G. Aad *et al.* (ATLAS Collaboration), *Observation of a new particle in the search for the Standard Model Higgs boson with the ATLAS detector at the LHC*, *Phys. Lett. B* **716** (2012) 1 [arXiv:1207.7214 [hep-ex]].

[8] S. Chatrchyan *et al.* (CMS Collaboration), *Observation of a new boson at a mass of 125 GeV with the CMS experiment at the LHC*, *Phys. Lett. B* **716** (2012) 30 [arXiv:1207.7235 [hep-ex]].

[9] G. Bertone, D. Hooper and J. Silk, *Particle dark matter: evidence, candidates and constraints*, *Phys. Rep.* **405** (2005) 279 [arXiv:hep-ph/0404175v2].

[10] A. Ahriche, *What is the criterion for a strong first order electroweak phase transition in singlet models?*, *Phys. Rev. D* **75** (2007) 083522 [arXiv:hep-ph/0701192v3].

[11] M. D'Onofrio and K. Rummukainen, *Standard model cross-over on the lattice*, *Phys. Rev. D* **93** (2016) 025003 [arXiv:arXiv:1508.07161v1 [hep-ph]].

[12] I. P. Ivanov, *Building and testing models with extended Higgs sector*, *Prog. Part. Nuc. Phys.* **95** (2017) 160 [arXiv:1702.03776 [hep-ph]].

[13] G. Branco, P. Ferreira, L. Lavoura, M. Rebelo, M. Sher and J. P. Silva, *Theory and phenomenology of two-Higgs-doublet models*, *Phys. Rep.* **516** (2012) 1 [arXiv:1106.0034 [hep-ph]].

[14] A. Djouadi, *The anatomy of electroweak symmetry breaking Tome II: The Higgs boson in the Minimal Supersymmetric Model*, *Phys. Rep.* **459** (2008) 1 [arXiv:hep-ph/0503173v2].

[15] A. Canepa, *Searches for supersymmetry at the Large Hadron Collider*, *Rev. Phys.* **4** (2019) 100033.

[16] L. Fromme, S. J. Huber and M. Seniuch, *Baryogenesis in the two-Higgs doublet model*, *J. High Energy Phys.* **2006** (2006) 038 [arXiv:0605242v2 [hep-ph]].

[17] M. J. Dugan, H. Georgi and D. B. Kaplan, *Anatomy of a composite Higgs model*, *Nucl. Phys. B* **254** (1985) 299.

[18] J. Mrazek, A. Pomarol, R. Rattazzi, M. Redi, J. Serra and A. Wulzer, *The other natural two Higgs doublet model*, *Nucl. Phys. B* **853** (2011) 1 [arXiv:1105.5403 [hep-ph]].

[19] S. De Curtis, L. D. Rose, S. Moretti and K. Yagyu, *A concrete composite 2-Higgs doublet model*, *J. High Energy Phys.* **12** (2018) 051 [arXiv:1810.06465 [hep-ph]].

[20] A. Sakharov, *Violation of CP invariance, C asymmetry, and baryon asymmetry of the universe*, *J. Exp. Theor. Fysik* **5** (1967) 32.

[21] P. Amaro-Seoane *et al.* (LISA Collaboration), *Laser Interferometer Space Antenna*, arXiv:1702.00786v3 [astro-ph.IM].

[22] Vincent Corbin and Neil J Cornish , *Detecting the cosmic gravitational wave background with the Big Bang Observer*, *Classical and Quantum Gravity* **23** (2006) 2435 [arXiv:gr-qc/0512039v1 [gr-qc]].

[23] Kawamura Seiji *et al.*, *The Japanese space gravitational wave antenna: DECIGO*, *Classical and Quantum Gravity* **28** (2011) 094011 [arXiv:gr-qc/0512039v1 [gr-qc]].

[24] J. Goldstone, A. Salam and S. Weinberg, *Broken symmetries*, *Phys. Rev.* **127** (1962) 965.

[25] I. F. Ginzburg and M. Krawczyk, *Symmetries of Two Higgs Doublet Model and CP violation*, *Phys. Rev. D* **72** (2005) 115013 [arXiv:hep-ph/0408011v3].

[26] D. Eriksson, J. Rathsman and O. Ståhl, *2HDMC - two-Higgs-doublet model calculator*, *Comput. Phys. Commun.* **181** (2009) 189 [arXiv:0902.0851 [hep-ph]].

[27] S. Davidson and E. H. Howard, *Basis-independent methods for the two-Higgs-doublet model*, *Phys. Rev. D* **72** (2005) 035004 [arXiv:hep-ph/0504050].

[28] H. E. Haber and D. O'Neil, *Basis-independent methods for the two-Higgs-doublet model. II. The significance of* $\tan\beta$, *Phys. Rev. D* **74** (2006) 015018 [arXiv:hep-ph/0602242v6].

[29] J. F. Gunion and H. E. Haber, *CP-conserving two-Higgs-doublet model: The approach to the decoupling limit*, *Phys. Rev. D* **67** (2003) 26.

[30] Peskin, Michael E. and Takeuchi, Tatsu, *New constraint on a strongly interacting higgs sector*, *Phys. Rev. Lett.* **65** (1990) 964.

[31] D. B. Kaplan, *Flavor at SSC energies: A New mechanism for dynamically generated fermion masses*, *Nucl. Phys. B.* **365** (1992) 259.

[32] E. Weinberg, *Radiative Corrections as the Origin of Spontaneous Symmetry Breaking*, `arXiv:hep-th/0507214v1`.

[33] S. De Curtis, S. Moretti, K. Yagyu and E. Yildirim, *Perturbative unitarity bounds in composite two-Higgs doublet models*, *Phys. Rev. D* **94** (2016) 055017 [`arXiv:1602.06437v2 [hep-ph]`].

[34] P. Basler and M. Mühlleitner, *BSMPT (Beyond the Standard Model Phase Transitions): A tool for the electroweak phase transition in extended Higgs sectors*, *Comput. Phys. Commun.* **237** (2019) 62 [`arXiv:1803.02846 [hep-ph]`].

[35] S. W. Ham and S. Oh, *Electroweak phase transition and Higgs self-couplings in the two-Higgs-doublet model*, `arXiv:hep-ph/0502116v1`.

[36] J. M. Cline, K. Kainulainen and M. Trott, *Electroweak Baryogenesis in Two Higgs Doublet Models and B meson anomalies*, *J. High Energy Phys.* **11** (2011) 089 [`arXiv:1107.3559v3 [hep-ph]`].

[37] M. Carrington, *Effective potential at finite temperature in the standard model*, *Phys. Rev. D* **45** (1992) 2933.

[38] M. Quiros, *Finite temperature field theory and phase transitions*, in *ICTP Summer School in High-Energy Physics and Cosmology*, pp. 187–259, 1999, `arXiv:hep-ph/9901312v1`.

[39] P. Arnold and O. Espinosa, *Effective potential and first-order phase transitions: Beyond leading order*, *Phys. Rev. D* **47** (1993) 3546 [`arXiv:hep-ph/9212235v2`].

[40] V. A. Rubakov and D. S. Gorbunov, *Introduction to the Theory of the Early Universe: Hot Big Bang Theory*. World Scientific, Singapore, 2:nd ed., 2018.

[41] R. R. Parwani, *Resummation in a hot scalar field theory*, *Phys. Rev. D* **45** (1992) 4695 [`arXiv:hep-ph/9204216v1`].

[42] C. L. Wainwright, *CosmoTransitions: Computing cosmological phase transition temperatures and bubble profiles with multiple fields*, *Comput. Phys. Commun.* **183** (2012) 2006 [`arXiv:1109.4189 [hep-ph]`].

[43] A. Ekstedt and J. Löfgren, *A critical look at the electroweak phase transition*, *J. High Energy Phys.* **136** (2020) [`arXiv:2006.12614v1 [hep-ph]`].

[44] J. M. Cline, K. Kainulainen and M. Trott, *Electroweak Baryogenesis in Two Higgs Doublet Models and B meson anomalies*, *J. High Energy Phys.* **11** (2011) 089 [arXiv:1107.3559v3 [hep-ph]].

[45] S. Coleman, *Fate of the false vacuum I: Semiclassical theory*, *Phys. Rev. D* **15** (1977) 2929.

[46] A. Linde, *Decay of the false vacuum at finite temperature.*, *Phys. Rev. D* **216** (1983) 421.

[47] M. E. Carrington and J. I. Kapusta, *dynamics of the electroweak phase transition*, *Phys. Rev. D* **47** (1993) 5304.

[48] C. Caprini, M. Hindmarsh, S. J. Huber, T. Konstandin, J. Kozaczuk, G. Nardini et al., *Science with the space-based interferometer eLISA. II: Gravitational waves from cosmological phase transitions*, arXiv:1512.06239v2 [astro-ph.CO].

[49] C. G. Callan and S. Coleman, *Fate of the false vacuum II: First quantum corrections*, *Phys. Rev. D* **16** (1977) 1762.

[50] C. Caprini, M. Chala, G. C. Dorsch, M. Hindmarsh, S. J. Huber, T. Konstandin et al., *Detecting gravitational waves from cosmological phase transitions with LISA: an update*, arXiv:1910.13125 [astro-ph.CO].

[51] M. Hindmarsh, S. J. Huber, K. Rummukainen and D. J. Weir, *Numerical simulations of acoustically generated gravitational waves at a first order phase transition*, *Phys. Rev. D* **92** (2015) 123008 [arXiv:1504.03291v2 [astro-ph.CO]].

[52] L. Husdal, *On Effectiev Degrees of Freedom in the Early Universe*, *Galaxies* **4** (2016) 78 [arXiv:1609.04979v3 [astro-ph.CO]].

[53] G. D. Moore and T. Prokopec, *Decay of the false vacuum at finite temperature.*, *Phys. Rev. D* **52** (1995) 7182 [arXiv:hep-ph/9506475v2].

[54] J. R. Espinosa, T. Konstandin, J. M. No and G. Servant, *Energy budget of cosmological first-order phase transitions.*, *JCAP* **06** (2010) 028 [arXiv:1004.4187v1 [hep-ph]].

[55] P. A. R. Ade *et al.* (Planck Collaboration), *Planck 2015 results. XIII. Cosmological parameters*, *Astron. Astrophys.* **594** (2016) [arXiv:1502.01589v3 [astro-ph.CO]].

[56] K. Schmitz, *New Sensitivity Curves for Gravitational-Wave Experiments*, arXiv:2002.04615v2 [hep-ph].

[57] H. Haber and O. Ståhl, *New LHC Benchmarks for the CP-conserving Two-Higgs-Doublet Model*, *Eur. Phys. J. C* **75** (2015) 491 [arXiv:1507.04281v4 [hep-ph]].

[58] I. Maksymyk, C. Burgess and D. London, *Beyond S, T, and U*, *Phys. Rev. D* **50** (1994) 529 [arXiv:hep-ph/9306267v3].

[59] M. Maniatis, A. von Manteuffel, O. Nachtmann and F. Nagel, *Stability and Symmetry Breaking in the General Two-Higgs-Doublet Model*, *Eur.Phys.J.C* **48** (2006) 805 [arXiv:hep-ph/0605184v2].

[60] I. F. Ginzburg and I. Ivanov, *Tree-level unitarity constraints in the most general 2HDM*, *Phys. Rev. D* **72** (2005) 115010 [arXiv:hep-ph/0508020v1].

[61] P. Bechtle, O. Brein, H. Sven, W. Georg and W. K. E, *HiggsBounds: Confirming arbitrary Higgs sectors with exclusion bounds from LEP and the Tevatron*, *Comput. Phys. Commun.* **181** (2010) 138 [arXiv:0811.4169v4 [hep-ph]].

[62] P. Bechtle, O. Brein, H. Sven, W. Georg and W. K. E, *HiggsBounds 2.0.0: Confronting neutral and charged Higgs sector predictions with exclusion bounds from LEP and the Tevatro*, *Comput. Phys. Commun.* **182** (2011) 2605 [arXiv:1102.1898v1 [hep-ph]].

[63] P. Bechtle, O. Brein, H. Sven, O. Ståhl and T. Stefaniak, *Recent Developments in HiggsBounds and a Preview of HiggsSignals*, *PoS* **CHARGED2012** (2013) 024 [arXiv:1301.2345v1 [hep-ph]].

[64] P. Bechtle, O. Brein, H. Sven, O. Ståhl and T. Stefaniak, *HiggsBounds-4: Improved Tests of Extended Higgs Sectors against Exclusion Bounds from LEP, the Tevatron and the LHC*, *Eur. Phys. J. C* **74** (2014) 2693 [arXiv:1311.0055v1 [hep-ph]].

[65] P. Bechtle, H. Sven, O. Ståhl, T. Stefaniak and G. Weiglein, *Applying Exclusion Likelihoods from LHC Searches to Extended Higgs Sectors*, *Eur. Phys. J. C* **75** (2015) 421 [arXiv:1507.06706v1 [hep-ph]].

[66] P. Bechtle, D. Dercks, T. Klingl, T. Stefaniak, G. Weiglein and J. Wittbrodt, *HiggsBounds-5: Testing Higgs Sectors in the LHC 13 TeV Era*, arXiv:2006.06007v1 [hep-ph].

[67] P. Bechtle, H. Sven, O. Ståhl, T. Stefaniak and G. Weiglein, *HiggsSignals: Confronting arbitrary Higgs sectors with measurements at the Tevatron and the LHC*, *Eur. Phys. J. C* **74** (2014) 2711 [arXiv:1305.1933v2 [hep-ph]].

[68] O. Ståhl and T. Stefaniak, *Constraining extended Higgs sectors with HiggsSignals*, *PoS* **EPS-HEP2013** (2014) 0314 [arXiv:arXiv:1310.4039v1 [hep-ph]].

[69] P. Bechtle, H. Sven, O. Ståhl, T. Stefaniak and G. Weiglein, *Probing the Standard Model with Higgs signal rates from the Tevatron, the LHC and a future ILC*, *J. High Energy Phys.* **11** (2014) 039 [arXiv:1403.1582v2 [hep-ph]].

[70] P. e. P. D. G. Zyla, *Review of Particle Physics*, *PTEP* **2020** (2020) 083C01 [arXiv:hep-ph/9306267v3].

[71] R. Enberg, J. Rathsman and G. Wouda, *Higgs phenomenology in the stealth doublet model*, *Phys. Rev. D* **91** (2015) 25 [arXiv:1311.4367v4 [hep-ph]].

[72] A. Freitas and J. Erler *Priv. Comm.* (2020) .

[73] F. Mahmoudi and O. Ståhl, *Flavor constraints on two-Higgs-doublet models with general diagonal Yukawa couplings*, *Phys. Rev. D* **81** (2010) 035016 [arXiv:0907.1791v2 [hep-ph]].

[74] *Ferrari method.*, *Encyclopedia of Mathematics.* (2014) .

[75] A. P. Morais and R. Pasechnik, *Probing multi-step electroweak phase transition with multi-peaked primordial gravitational waves spectra*, arXiv:1910.00717v3 [hep-ph].

[76] J. Rathsman *Priv. Comm.* (2020) .

[77] J. e. Alison, *Higgs boson potential at colliders: Status and perspectives*, *Rev. Phys.* **5** (2020) 100045 [arXiv:1910.00012 [hep-ph]].